

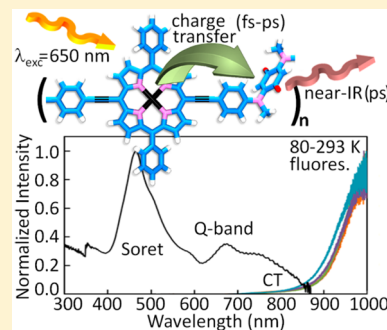
Push–Pull Porphyrin-Containing Polymers: Materials Exhibiting Ultrafast Near-IR Photophysics

Xiaorong Wang, Gessie Brisard, Daniel Fortin, Paul-Ludovic Karsenti, and Pierre D. Harvey*

*Département de chimie, Université de Sherbrooke, Sherbrooke, Québec J1K 2R1, Canada

Supporting Information

ABSTRACT: Four push–pull polymers of structure $(\text{C}\equiv\text{C}-[\text{Zn}]-\text{C}\equiv\text{C}-\text{A})_n$ (A = isoindigo (**P1**), bis(α -methylamino-1,4-benzene)quinone (**P2**), 2-(*N*-methylamino-1,4-benzene)-*N*-1,4-benzene-maleimide (**P3**), and 2,2'-anthraquinone (**P4**); $[\text{Zn}]$ = [bis(*meso*-aryl)porphyrin]zinc(II) = donor) and models **M1** and **M2** ($\text{A}'-\text{C}\equiv\text{C}-[\text{Zn}]-\text{C}\equiv\text{C}-\text{A}'$; A' = respectively naphthoquinone and 2-anthraquinone) were prepared and characterized (^1H and ^{13}C NMR, elemental analysis, GPC, TGA, cyclic voltammetry, steady state and ultrafast time-resolved UV–vis and emission spectroscopy) and studied by density functional theory (DFT) and time-dependent DFT (TDDFT) in order to address the nature of the low-lying singlet and triplet excited states. **P1** (fully conjugated polymer), **P2** (formally nonconjugated but exhibit strong electronic communication across the chain) and **P4** (formally nonconjugated but local conjugation between the donor and acceptor) are near-IR emitters ($\lambda_{\text{max}} > 750 \text{ nm}$). **M1** and **M2** are mono- $\text{C}\equiv\text{C}-[\text{Zn}]-\text{C}\equiv\text{C}$ species, and **P3** exhibits a very modest CT contribution (as maleimide is a weak acceptor) and are not near-IR emitters. The nature of the S_1 and T_1 excited states are CT processes donor* \rightarrow acceptor. In **P1–P4**, a dual fluorescence ($7.7 < \tau_{\text{F}} < 770 \text{ ps}$; except one value at 2.5 ns; **P3**) is depicted, which are assigned to fluorescences arising from the terminal and central units of the polymers identified from the comparison with **M1** and **M2**. The high and low energy fluorescences are respectively short ($77 < \tau_{\text{F}} < 166 \text{ ps}$) and long-lived ($688 < \tau_{\text{F}} < 765 \text{ ps}$) suggesting S_1 energy transfers with rates, k_{ET} , of 7.1 (**P1**), 12 (**P2**) and 4.5 (ns)^{-1} (**P4**). The fs transient absorption spectra exhibit particularly very short triplet lifetimes ($2.3 < \tau_{\text{T}} < 87 \text{ ns}$) explaining the absence of phosphorescence. Also ultrafast lifetimes ($85 < \tau < 1290 \text{ fs}$) for species excited in the 0–0 peak of the Q-band (650 nm; i.e., $\pi\pi^*$ porphyrin level) indicating its rather efficient nonradiative deactivation ($\text{S}_n \sim > \text{S}_1$ and $\text{S}_n \sim > \text{T}_m$). When cooling takes place or the solution concentration is increased, new red-shifted fluorescence bands appear, evidencing aggregate formation. Both fluorescence and transient absorption lifetimes of **P1–P4** become shorter and their band intensity lower. Finally, the position of the optically silent phosphorescence has been predicted to be in the 1300 (**P1**, **P2**) and 1000 nm (**P3**, **P4**) zones (DFT).



INTRODUCTION

Conjugated push–pull polymers have been the topic of intense research over the past decade or so, namely for the design of new materials for photovoltaic cells.¹ One of the chromophores that received little attention relative to thiophene, phenylenevinylene, pyrrole, and structurally related units (this list is not exhaustive), is the porphyrin. Several conjugated polyporphyrins have been reported so far, including a few push–pull examples,² along with their low band gap properties. Generally, the metalloporphyrin unit plays the role of the donor residue. We find surprising that the known acceptor isoindigo (2*H*-indol-2-one, 3-(1,2-dihydro-1-alkyl-2-oxo-3*H*-indol-3-ylidene)-1,3-dihydro-1-alkyl)^{3–5} was not used as a potential acceptor except for one work reported by Therien and collaborators, who investigated a monomer composed of one zinc(II)porphyrin conjugated with two *meso*-isoindigo units.^{4a} Similarly, the spacer 2,2'-anthraquinone, which appears as a nonconjugated unit, was recently reported to form a “push–pull” organometallic polymer of Pt(II),⁶ but no polymer containing porphyrin was reported so far. In fact, only a dimer of nickel(II) porphyrin was studied.⁷ Interestingly in this case,

electrochemical results indicate that the two units are coupled (i.e., presence of electronic communication). Finally, the bis(*p*-phenylethynyl)quinone diimine and its related derivatives in relation with polyaniline were also the subject of intense investigations by our group toward the design of polymers,⁸ and only two polymers containing a porphyrin donor was reported (see **PSa,b** in Chart 1).⁹ Facing this obvious paucity of porphyrin-containing push–pull polymers (i.e., only 2 cases of the same type),¹⁸ we were intrigued by the design of other related examples along with their optical and electronic properties whether they are formally conjugated (like in isoindigo) or not (like in 2,2'-anthraquinone), in comparison with those using the bis(*p*-phenylethynyl)quinone diimine acceptor (here conjugated).

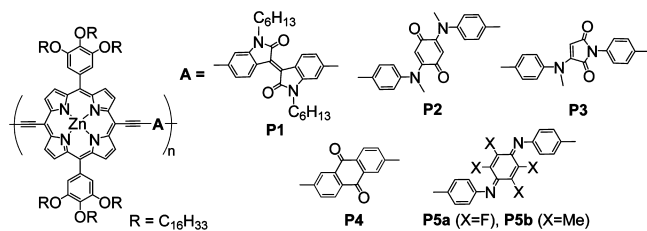
We now wish to report the synthesis and properties of push–pull polymers containing the bis[*meso*-(ethynyl)zinc(II)] porphyrin, $\text{C}\equiv\text{C}-[\text{Zn}]-\text{C}\equiv\text{C}$, as the donor unit and the

Received: July 19, 2015

Revised: September 5, 2015



Chart 1. Structures of the Push–Pull Porphyrin-Containing Polymers Investigated in This Work (P1–P4) in Comparison with That for P5a,b



isoindigo,^{3–5} bis(α -methylamino-1,4-benzene)quinone,¹⁰ *N*-(1,4-benzene) (methylamino-1,4-benzene) maleimide,^{10c,11} and 2,2'-anthraquinone^{6,7} as acceptors (see respectively structures **P1–P4**, in **Chart 1**). The three latter acceptors are formally unconjugated but recent studies unambiguously demonstrate that these materials exhibit electronic communication across the units.^{7,10c} Evidence for S_1 energy transfer (terminal* \rightarrow central units) is also provided for the near-IR emitters **P1**, **P2**, and **P4** ($\lambda_{\text{max}} > 750$ nm). All photophysical parameters also demonstrate that the S_n excited state deactivations are ultrafast.

EXPERIMENTAL SECTION

Materials. 5,15-Bis(3,4,5-tris(cetyloxy)phenyl)porphyrin,¹² (*E*)-6,6'-dibromo-1,1'-dihexyl-[3,3'-biindolinylidene]-2,2'-dione (**2**),¹³ 2,5-bis((4-iodophenyl) (methyl)amino)cyclohexa-2,5-diene-1,4-dione (**3**),^{10c} 2,6-dibromo-9,10-anthraquinone (**4**),¹⁴ 1-(4-ethynylphenyl)-3-((4-ethynylphenyl) (methyl)amino)-1*H*-pyrrole-2,5-dione (**7**),^{10c} and 2-ethynylanthracene-9,10-dione (**8**),¹⁵ were prepared according to literature procedures. Compound **5** was obtained by using the same method as **3**. All reactions were performed in Schlenk-tube flasks under purified nitrogen. All flasks were dried under a flame to eliminate moisture. All solvents were distilled from appropriate drying agents. All other reagents were used as received.

[5,15-Dibromo-10,20-bis(3,4,5-tris(cetyloxy)phenyl)porphyrinato]zinc(II) (**6**). 5,15-Bis(3,4,5-tris(cetyloxy)phenyl)porphyrin (800 mg, 0.42 mmol) was dissolved in chloroform (150 mL), and pyridine (0.4 mL) was added. The reaction mixture was cooled to 0 °C and NBS (*N*-bromosuccinimide) (150 mg, 0.84 mmol) was added. After being stirred for 0.5 h, the mixture was allowed to warm up to room temperature and stirred for 4 h. The reaction was quenched by addition of acetone (5 mL). Zn(OAc)₂·H₂O (75 mg, 1 mmol) in methanol (15 mL) was added into the solution above. The reaction mixture was stirred at room temperature for 2 h. The evaporation of the solvent and purification by column chromatography (silica gel, CH₂Cl₂/hexanes (1/1)) afforded a purple solid (800 mg, 90% yield). ¹H NMR (400 MHz, CDCl₃): δ (ppm) 9.73 (d, *J* = 4.8 Hz, 4 H), 9.06 (d, *J* = 4.8 Hz, 4 H), 7.36 (s, 4 H), 4.29 (t, *J* = 6.4 Hz, 4 H), 4.09 (t, *J* = 6.4 Hz, 8 H), 1.97 (m, 4 H), 1.87 (m, 8 H), 1.67 (m, 4 H), 1.47 (m, 8 H), 1.25 (m, 144 H), 0.87 (m, 18 H). ¹³C NMR (101 MHz, CDCl₃): δ 151.25, 151.17, 150.43, 138.08, 137.09, 133.91, 133.40, 122.68, 114.51, 105.49, 73.95, 69.52, 32.19, 32.15, 30.79, 30.14, 30.11, 30.08, 30.03, 30.01, 29.93, 29.88, 29.69, 29.67, 29.65, 29.59, 26.54, 26.35, 22.95, 22.92, 14.38, 14.36. MS (MALDI–TOF): *m/z* 2126 (M^+). Anal. Calcd for C₁₂₈H₂₁₀Br₂N₄O₆Zn: C, 72.30; H, 9.95; N, 2.64. Found: C, 71.97; H, 9.56; N, 2.50%.

[5,15-Diethynyl-10,20-bis(3,4,5-tris(cetyloxy)phenyl)porphyrinato]zinc(II) (**1**). Compound **6** (800 mg, 0.38 mmol) was dissolved in THF (75 mL), and triethylamine (75 mL) was added. The mixture was purged with nitrogen for 30 min. Pd(PPh₃)₂Cl₂ (13 mg, 0.02 mmol), CuI (4 mg, 0.02 mmol), and trimethylsilylacetylene (0.2 mL, 1.14 mmol) were added. After heating at 60 °C for 48 h under nitrogen, the solvent was removed under reduced pressure. The residue was filtered using CH₂Cl₂ over a silica carpet. The filtrate was collected and evaporated to 100 mL, and tetrabutylammonium

fluoride (1 mL, 1 M in THF) was added. After stirring for 2 h, water was added to quench the reaction. The solution was extracted with chloroform, washed with water and dried over anhydrous MgSO₄. After evaporation of the solvent, the residue was purified by column chromatography (silica gel, CH₂Cl₂/hexanes (1/1)) to give a green solid (500 mg, 66% yield). ¹H NMR (400 MHz, CDCl₃): δ (ppm) 9.72 (d, *J* = 4.8 Hz, 4 H), 9.05 (d, *J* = 4.4 Hz, 4 H), 7.38 (s, 4 H), 4.27 (t, *J* = 6.4 Hz, 4 H), 4.18 (s, 2 H), 4.09 (t, *J* = 6.4 Hz, 8 H), 1.95 (m, 4 H), 1.88 (m, 8 H), 1.67 (m, 4 H), 1.47 (m, 8 H), 1.26 (m, 144 H), 0.86 (m, 18 H). ¹³C NMR (101 MHz, CDCl₃): δ 152.50, 151.31, 150.61, 138.03, 137.10, 133.27, 131.40, 122.93, 114.42, 100.32, 85.98, 84.28, 73.93, 69.52, 32.19, 32.15, 30.80, 30.15, 30.11, 30.08, 30.06, 30.02, 30.02, 29.94, 29.88, 29.70, 29.65, 29.59, 26.55, 26.37, 22.95, 22.92, 14.38, 14.36. MS (MALDI–TOF): *m/z* 2018 ($M + 1$). Anal. Calcd for C₁₃₂H₂₁₂N₄O₆Zn: C, 78.62; H, 10.60; N, 2.78. Found: C, 78.30; H, 10.28; N, 2.39%.

Bis(2-(methyl(phenyl)amino)naphthalene-1,4-dione)[(5,15-diethynyl-10,20-bis(3,4,5-tris(cetyloxy)phenyl)porphyrinato]zinc(II) (**M1**). A 100 mg quantity (0.05 mmol) of **1**, 38.9 mg (0.10 mmol) of **5**, 3 mg (0.003 mmol) of Pd₂(dba)₃ (dba = dibenzylidene-acetone), and 23 mg (0.075 mmol) of AsPh₃ were dissolved in THF (50 mL) and Et₃N (50 mL), and the reaction was stirred at 45 °C for 48 h under argon. The solvent was evaporated, and the residue was purified by column chromatography using CH₂Cl₂/hexane (1:1, v/v) as the eluent to give **M1** (68 mg, 54% yield) as a deep green solid. ¹H NMR (400 MHz, CDCl₃): δ (ppm) 9.62 (d, *J* = 4.0 Hz, 4 H), 8.91 (d, *J* = 4.4 Hz, 4 H), 7.87 (d, *J* = 8.0 Hz, 4 H), 7.62 (br, 4 H), 7.35 (br, 4 H), 7.14 (m, 4 H), 6.87 (br, 4 H), 4.98 (s, 1 H), 4.20 (m, 4 H), 4.00 (m, 8 H), 3.23 (s, 6 H), 1.88–1.77 (br, 12H), 1.41–1.39 (br, 12 H), 1.15–1.08 (br, 144 H), 0.76–0.68 (m, 18 H). ¹³C NMR (101 MHz, CDCl₃): δ 183.69, 181.56, 152.26, 151.44, 150.43, 148.09, 138.15, 137.50, 133.94, 133.01, 132.70, 131.95, 131.80, 130.94, 126.74, 125.51, 125.37, 123.24, 121.98, 114.49, 112.65, 101.69, 96.43, 93.91, 74.04, 69.68, 43.11, 32.14, 30.90, 30.12, 30.05, 30.03, 29.94, 29.58, 26.47, 22.91, 14.35. MALDI–TOF: 2540 ($M + 1$). Anal. Calcd for (C₁₆₆H₂₃₄N₆O₁₀Zn)n: C, 78.52; H, 9.29; N, 3.31. Found: C, 78.15; H, 9.48; N, 3.58%.

Bis(2-anthraquinone)[(5,15-diethynyl-10,20-bis(3,4,5-tris(cetyloxy)phenyl)porphyrinato]zinc(II) (**M2**). A 212.7 mg quantity (0.1 mmol) of **6**, 46.4 mg (0.2 mmol) of **8**, 3.5 mg (0.005 mmol) Pd(PPh₃)₂Cl₂, and 1 mg (0.005 mmol) of CuI were dissolved in THF (50 mL) and Et₃N (50 mL). The reaction was stirred at 65 °C for 24 h under nitrogen. The solvent was evaporated, and the residue was purified by column chromatography using CH₂Cl₂/hexane (1:1, v/v) as the eluent to give **M2** (170 mg, 70% yield) after recrystallization (CHCl₃/acetone) as a green solid. ¹H NMR (400 MHz, CDCl₃): δ (ppm) 9.50 (s, 4 H), 9.10 (s, 4 H), 7.65 (s, 4 H), 7.53–7.27 (br, 14 H), 4.47 (br, 4 H), 4.35 (br, 8 H), 2.05 (br, 12 H), 1.55–1.19 (br, 156 H), 0.90–0.81 (br, 18 H). MS (MALDI–TOF): *m/z* 2428 ($M + 1$). Anal. Calcd for C₁₆₀H₂₂₄N₄O₁₀Zn: C, 79.12; H, 9.30; N, 2.31. Found: C, 79.41; H, 9.57; N, 2.52%.

Poly(1,1'-dihexyl-[3,3'-biindolinylidene]-2,2'-dione)[(5,15-diethynyl-10,20-bis(3,4,5-tris(cetyloxy)phenyl)porphyrinato]zinc(III) (**P1**). A 100 mg quantity (0.05 mmol) of **1**, 29.4 mg (0.05 mmol) of **2**, 3 mg (0.003 mmol) of Pd₂(dba)₃, and 23 mg (0.075 mmol) of AsPh₃ were dissolved in THF (50 mL) and Et₃N (50 mL), and the reaction was stirred at 45 °C for 48 h under argon. The solvent was evaporated and the residue was purified by column chromatography using CH₂Cl₂/hexane (1:1, v/v) as the eluent to give **P1** (78 mg, 64% yield) as a deep green solid. ¹H NMR (400 MHz, CDCl₃): δ (ppm) 9.09 (br, 6 H), 7.50 (br, 6 H), 6.93 (br, 6 H), 4.36 (br, 4 H), 4.17 (br, 8 H), 3.50 (br, 4 H), 1.93 (br, 12 H), 1.26 (br, 172 H), 0.89 (br, 24 H).

Poly((2,5-bis(methyl(phenyl)amino)cyclohexa-2,5-diene-1,4-dione)[(5,15-diethynyl-10,20-bis(3,4,5-tris(cetyloxy)phenyl)porphyrinato]zinc(III) (**P2**). A 100 mg quantity (0.05 mmol) of **1**, 28.5 mg (0.05 mmol) of **3**, 3 mg (0.003 mmol) of Pd₂(dba)₃, and 23 mg (0.075 mmol) of AsPh₃ were dissolved in THF (50 mL) and Et₃N (50 mL). The reaction was stirred at 45 °C for 48 h under Ar. The solvent was evaporated, and the residue was purified by column chromatography using CH₂Cl₂/hexane (1:1, v/v) as the eluent to give **P2** (70 mg, 60% yield) as a deep green solid. ¹H NMR (400 MHz, CDCl₃): δ

(ppm) 9.75 (br, 4 H), 9.05 (br, 4 H), 7.99 (br, 2 H), 7.66 (br, 2 H), 7.42 (br, 6 H), 6.85 (br, 4 H), 4.32 (br, 4 H), 4.12 (br, 8 H), 3.40 (br, 6 H), 1.93 (br, 12 H), 1.41–1.21 (br, 168 H), 0.85 (br, 18 H).

Poly((3-(methyl(phenyl)amino)-1-phenyl-1H-pyrrole-2,5-dione)-[(5,15-diethynyl-10,20-bis(3,4,5-tris(cetyloxy)phenyl)porphyrinato]zinc(II)) (P3). A 100 mg quantity (0.05 mmol) of **1**, 16.3 mg (0.05 mmol) **7**, 3.5 mg (0.005 mmol) Pd(PPh₃)₂Cl₂, and 1 mg of CuI (0.005 mmol) were dissolved in THF (50 mL) and Et₃N (50 mL). The reaction was stirred at 65 °C for 48 h under argon. The solvent was evaporated, and the residue was purified by column chromatography using CH₂Cl₂/hexane (1:1, v/v) as the eluent to give **P3** (48 mg, 42% yield) as a green solid. ¹H NMR (400 MHz, CDCl₃): δ (ppm) 9.76 (br, 4 H), 9.07 (br, 4 H), 8.11 (br, 2 H), 7.57 (br, 4 H), 7.41 (br, 6 H), 5.27 (br, 1 H), 4.32 (br, 4 H), 4.12 (br, 8 H), 3.57 (br, 3 H), 1.98–1.89 (br, 12 H), 1.41–1.21 (br, 156 H), 0.86 (br, 18 H).

Poly((2-anthraquinone)[(5,15-diethynyl-10,20-bis(3,4,5-tris(cetyloxy)phenyl)porphyrinato]zinc(II)) (P4). A 100 mg (0.05 mmol) of **1**, 18.3 mg (0.05 mmol) of **4**, 3 mg (0.003 mmol) of Pd₂(dba)₃, and 23 mg (0.075 mmol) of AsPh₃ were dissolved in THF (50 mL) and Et₃N (50 mL). The reaction was stirred at 65 °C for 48 h under argon. The solvent was evaporated and the residue was purified by column chromatography using CH₂Cl₂/hexane (1:1, v/v) as the eluent to give **P4** (101 mg, 85% yield) as a deep green solid. ¹H NMR (400 MHz, CDCl₃): δ (ppm) 9.25–8.99 (br, 4 H), 8.36 (d, J = 2.0 Hz, 2 H), 8.08 (d, J = 8.4 Hz, 4 H), 7.89 (dd, J = 8.0, 2.0 Hz, 4H), 7.27 (s, 4 H), 4.57–4.25 (br, 12 H), 1.50–0.79 (br, 186 H).

2,5-Bis(4-bromoaniline)quinone Diamine (9a). 4-Bromoaniline (1.0 g, 6.0 mmol) was dissolved in 100 mL of absolute ethanol, and 1,4-benzoquinone (0.22 g, 2.0 mmol) was added while bubbling oxygen through the solution for 12 h. A precipitate formed which was filtered through a Buchner funnel and washed with cold absolute ethanol. The brown product (0.27 g, 30% yield) was placed in the oven at 100 °C prior to be dried under vacuum. IR (KBr)/cm⁻¹ ν: 3237 (N–H). ¹H NMR (400 MHz, DMSO): δ (ppm) 9.38 (s, 2 H, NH), 7.60 (s, 4 H, CH arom), 7.35 (s, 4 H, CH arom); 5.82 (s, 2 H, H-quinone). *m/z* (EI): 448 (M⁺).

2,5-Bis(4-(trimethylsilyl)ethynylaniline)quinone Diamine (10a). 2,5-Bis(4-bromoaniline)quinone diamine (1.0 g, 4.0 mmol) was dissolved in a solvent mixture (40 mL of toluene and 15 mL of diisopropylamine), containing 0.10 g (0.40 mmol) of PPh₃, 0.14 g (0.20 mmol) of PdCl₂(PPh₃)₂ and 0.040 g (0.20 mmol) of CuI and was stirred under argon for 30 min. Using a syringe, ethynyltrimethylsilane (1.0 mL, 8.0 mmol) was added dropwise. The solution was heated at 90 °C for 12 h. The solvent was evaporated and the product was dissolved in CHCl₃, washed with water (3 × 30 mL) and dried over anhydrous MgSO₄. The red product (0.35 g, 36% yield) was purified using silica chromatography with CHCl₃ as the solvent. IR (KBr)/cm⁻¹ ν: 3270 (N–H), 2158 (C≡C). ¹H NMR (400 MHz, CDCl₃): δ (ppm) 8.11 (2 H, s, NH), 7.50 (4 H, m, CH aro), 7.20 (4 H, m, CH aro), 6.13 (2 H, s, H-Quinone), 0.25 (18 H, s, Si(CH₃)₃). ¹³C NMR (101 MHz, CDCl₃): δ 180.34, 145.47, 137.22, 133.39, 121.81, 120.55, 104.15, 96.84, 95.42, 0.00. *m/z* (EI): 482 (M⁺).

Di-tert-butyl (3,6-Dioxocyclohexa-1,4-diene-1,4-diyl)bis(4-iodophenyl)carbamate (10b). To a solution of **10a** (1.02 g, 2 mmol) in THF was added BOC₂O (1.66 g, 7.6 mmol). This solution was stirred at room temperature for 12 h after the addition of 4-dimethylaminopyridine (DMAP, 0.244 g, 2 mmol). The solvent was evaporated. The crude product was purified by chromatography on silica gel using CH₂Cl₂/hexane (1:1, v/v) to give **10b** (0.78 g, 53% yield) as a yellow solid. ¹H NMR (400 MHz, CDCl₃): δ (ppm) 7.68 (d, J = 8.4 Hz, 4 H, Ar), 6.94 (d, J = 8.4 Hz, 4 H, Ar), 6.38 (s, 2 H, Ar), 1.43 (s, 18 H, 6CH₃). ¹³C NMR (101 MHz, CDCl₃): δ 182.32, 152.35, 148.22, 140.98, 138.71, 128.92, 127.04, 92.54, 83.79, 28.09 ppm. ESI–Tof: *m/z* calculated, 764.9929 (MNa⁺); *m/z* observed, 764.9929 (MNa⁺).

Instruments. The ¹H and ¹³C NMR spectra were collected on a Bruker DRX400 spectrometer using the solvent as chemical shift standard. The coupling constant are in Hz. MALDI–TOF mass spectra were recorded on a Bruker BIFLEX III TOF mass spectrometer (Bruker Daltonics, Billerica, MA, USA) using a 337

nm nitrogen laser with dithranol as matrix. The spectra were measured from freshly prepared samples. The molecular weights of the polymers were determined by GPC (HP 1050 series HPLC with visible wavelength and fluorescent detectors) using polystyrene standards and THF as an eluent, and the thermal analyses were performed with the PerkinElmer TGA6 thermal analyzer. The absorption spectra in the solution were measured on a Varian Cary 300 Bio UV–vis spectrometer at 298 K and on a Hewlett-Packard 8452A diode array spectrometer with a 0.1 s integration time at 77 K. The solid state spectra were measured by forming a polymer film on the microscope slide and were measured on a Varian Cary 300 Bio UV–vis spectrometer at 298 K. The steady state fluorescence (<820 nm) and the corresponding excitation spectra were acquired on an Edinburgh Instruments FLS980 phosphorimeter equipped with single monochromators. Fluorescence lifetime measurements were made with the FLS908 spectrometer using a 378 nm picosecond pulsed diode laser (fwhm = 78 ps) as an excitation source. Data collection on the FLS980 system was performed by time correlated single photon counting (TCSPC). The emission spectra located in the near-IR region and the corresponding excitation spectra were recorded on a PTI QM-400 instrument. All fluorescence spectra were corrected for instrument response.

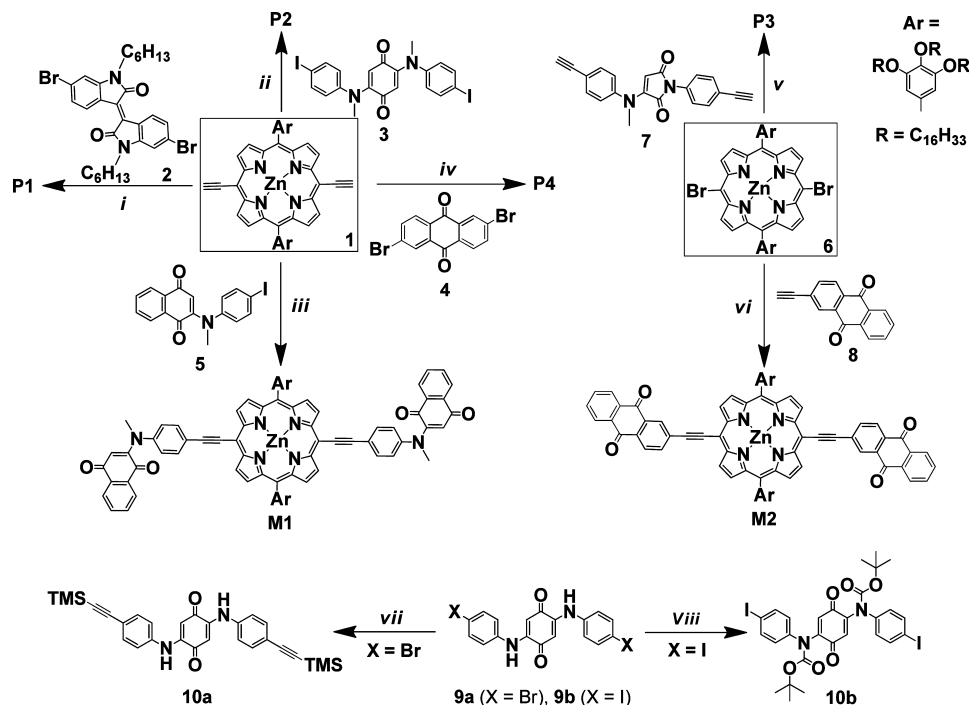
Electrochemistry. The electrochemical measurements were carried out using a standard three-electrode configuration (Pt working electrode, a platinum counter electrode and a Ag wire as a pseudoreference electrode) and a PARC 273A potentiostat interfaced to a personal computer at room temperature under a flow of nitrogen gas. The solvent in all measurements was deoxygenated THF, and the supporting electrolyte was 0.1 M [Bu₄N]⁺[PF₆]⁻. The ferrocenium/ferrocene (FcP₂⁺⁰) couple was used as a standard, the reference electrode was calibrated at the end of each experiment against the ferrocene/ferrocenium couple (Fc/Fc⁺), whose formal potential is 0.56 V, relative to the KCl saturated calomel electrode (SCE).¹⁶

Femtosecond Transient Absorption Spectroscopy. The fs transient spectra and decay profiles were acquired on a homemade system using the SHG of a Soltice (Spectra Physics) Ti–sapphire laser (λ_{exc} = 398 nm; fwhm >75 fs; pulse energy = 0.1 μJ per pulse, rep. rate = 1 kHz; spot size ~500 μm), a white light continuum generated inside a sapphire window and a custom-made dual CCD camera of 64 × 1024 pixels sensitive between 200 and 1100 nm (S7030, Spectronic Devices). The delay line permitted to probe up to 4 ns with an accuracy of ~4 fs. The results were analyzed with the program Glotaran (<http://glotaran.org>) permitting one to extract a sum of independent exponentials (I(λ,t) = C₁(λ) × e^{-t₁/τ} + C₂(λ) × e^{-t₂/τ} + ...) that fits the whole 3D transient map.

Fast Kinetic Fluorescence Measurements. The short components of the fluorescence decays were measured using the output of an OPA (OPA-800CF, SpectraPhysics) operating at λ_{exc} = 490 nm, a pulse width of 90 fs, rep. rate = 1 kHz, pulse energy = 1.6 μJ per pulse, spot size ~2 mm, and a Streak camera (Axis-TRS, Axis Photonique Inc.) with less than 8 ps resolution. The results were also globally analyzed with the program Glotaran (<http://glotaran.org>) permitting one to extract a sum of independent exponentials (I(λ,t) = C₁(λ) × e^{-t₁/τ} + C₂(λ) × e^{-t₂/τ} + ...).

Quantum Yield Measurements. For room-temperature measurements, all samples were prepared under an inert atmosphere (in a glovebox, O₂ < 12 ppm) by dissolution of the different compounds in THF using 1 cm³ quartz cells with septum (298 K) measurements. Three different measurements (i.e., different solutions) were performed for each set of photophysical data (quantum yield). The sample concentrations were chosen to correspond to an absorbance of 0.05 at the excitation wavelength. Each absorbance value was measured three times for better accuracy in the measurements of emission quantum yield. The reference was tetraphenylporphyrin (Φ_F = 0.11).¹⁷

X-ray Crystallography. The crystals of **10a** were grown by slow evaporation of CH₂Cl₂ at room temperature. One single crystal of 0.02 × 0.25 × 0.40 mm³ was mounted using a glass fiber at 298(2) K on the goniometer. Data were collected on an Enraf-Nonius CAD-4 automatic diffractometer at the Université de Sherbrooke using ω scans. The DIFRAC¹⁸ program was used for centering, indexing, and

Scheme 1. Synthesis of P1, P2, P3, P4, M1, M2, 10a, and 10b^a

^aKey: (i) THF/Et₃N, AsPh₃, Pd₂(dba)₃, 45°C, 48 h; (ii) THF/Et₃N, AsPh₃, Pd₂(dba)₃, 45°C, 48 h; (iii) THF/Et₃N, AsPh₃, Pd₂(dba)₃, 45°C, 48 h; (iv) THF/Et₃N, AsPh₃, Pd₂(dba)₃, 65°C, 48 h; (v) THF/Et₃N, CuI, Pd(PPh₃)₂Cl₂, 65°C, 48 h; (vi) THF/Et₃N, CuI, Pd(PPh₃)₂Cl₂, 65°C, 24 h; (vii) toluene/Et₃N, CuI, PPh₃, Pd(PPh₃)₂Cl₂, ethynyltrimethylsilane, 90°C, 12 h; (viii) THF, DMAP, BOC₂O, 5 h.

data collection. One standard reflection was measured every 100 reflections, no intensity decay was observed during data collection. The data were corrected for absorption by empirical methods based on psi scans and reduced with the NRCVAX¹⁹ programs. They were solved using SHELXS-97²⁰ and refined by full-matrix least-squares on F^2 with SHELXL-97.²⁰ The non-hydrogen atoms were refined anisotropically. The hydrogen atoms were placed at idealized calculated geometric position and refined isotropically using a riding model. The crystal plates were very thin with a face of only 0.02 mm making the diffraction % observed low.

The crystals of **10b** were grown by slow evaporation of a CHCl₃/CH₃OH solution. A clear light orange Plate-like specimen of C₂₈H₂₈I₂N₂O₆, approximate dimensions 0.030 mm × 0.360 mm × 0.670 mm, was used for the X-ray crystallographic analysis. The X-ray intensity data were measured on a Bruker Kappa APEX II DUO CCD system equipped with a TRIUMPH curved-crystal monochromator and a Mo fine-focus tube ($\lambda = 0.71073$ Å). A total of 1091 frames were collected. The total exposure time was 2.42 h. The frames were integrated with the Bruker SAINT software package using a narrow-frame algorithm. The integration of the data using a triclinic unit cell yielded a total of 6907 reflections to a maximum θ angle of 26.57° (0.79 Å resolution), of which 6907 were independent (average redundancy 1.000, completeness = 92.6%, $R_{\text{sig}} = 5.78\%$) and 6692 (96.89%) were greater than $2\sigma(F^2)$. The final cell constants of $a = 6.1385(11)$ Å, $b = 9.4691(17)$ Å, $c = 25.004(5)$ Å, $\alpha = 88.849(5)^\circ$, $\beta = 88.489(5)^\circ$, $\gamma = 81.113(5)^\circ$, volume = 1435.2(4) Å³, are based upon the refinement of the XYZ-centroids of 9950 reflections above $20\sigma(I)$ with $4.674^\circ < 2\theta < 53.14^\circ$. Data were corrected for absorption effects using the multiscan method (SADABS). The ratio of minimum to maximum apparent transmission was 0.701. The calculated minimum and maximum transmission coefficients (based on crystal size) are 0.3174 and 0.9363. The structure was solved and refined using the Bruker SHELXTL Software Package, using the space group $P1$, with $Z = 2$ for the formula unit, C₂₈H₂₈I₂N₂O₆. The final anisotropic full-matrix least-squares refinement on F^2 with 326 variables converged at $R1 = 8.98\%$, for the observed data and $wR2 = 23.96\%$ for all data. The goodness-of-fit was 1.130. The largest peak in the final difference

electron density synthesis was $9.412 \text{ e}^-/\text{\AA}^3$ and the largest hole was $-6.927 \text{ e}^-/\text{\AA}^3$ with an RMS deviation of $0.359 \text{ e}^-/\text{\AA}^3$. On the basis of the final model, the calculated density was 1.718 g/cm^3 and $F(000)$, 728 e⁻.

Computations. Calculations were performed with Gaussian 09²¹ at the Université de Sherbrooke with Mammouth supercomputer supported by le Réseau Québécois de Calculs de Haute Performances. The DFT^{22–25} and TDDFT^{26–28} were calculated with the B3LYP^{29–31} method. 6-31G*^{32–37} basis sets were used for C, H, N, and O atoms, and VDZ (valence double ζ) with SBKJJC effective core potentials^{38–40} were used for Zn atoms. The calculated absorption spectra and related MO contributions were obtained from the TDDFT/singlets output file and gausssum2.2.⁴¹ The electrode potentials and orbital energies were obtained from the DFT calculations with a method like Namazian et al.⁴² The model compounds were optimized before the time-dependent density-functional theory (TDDFT) calculations. Only the relevant (stronger oscillator strength and wave function coefficients) molecular orbitals are shown. All computations were performed without symmetry constraints. The predicted phosphorescence wavelengths were obtained by calculating the difference in the total energy between the optimized triplet state and the optimized singlet state. This energy difference is equated to the T_1-S_0 gap and can therefore be used to predict the phosphorescence wavelength of a compound.⁴³

RESULTS AND DISCUSSION

Synthesis and Characterization. The syntheses of model compounds **10a**, **10b**, **M1** and **M2** and polymers **P1**, **P2**, **P3** and **P4** are shown in Scheme 1.

First, the starting material **1** (HC≡C-[Zn]-C≡CH) was synthesized from a Sonogashira coupling of **6** (Br-[Zn]-Br) with Me₃SiC≡CH, followed by the deprotection of the ethynyls with Bu₄NF. **M1**, **P1**, **P2**, and **P4** were obtained by free Cu(I) Sonogashira coupling reaction between **1** and respectively **5**, **2**,¹⁵ **3**,^{10c} and **4**¹⁴ separately. Concurrently, **M2**

and **P3** were prepared from compound **6** with **7**,^{10c} **8**¹⁵ by Sonogashira coupling using Pd(PPh₃)₂Cl₂/CuI as catalysts. The model **10a** was prepared from a Sonogashira coupling of **9a** with Me₃SiC≡CH, whereas model **10b** was obtained from the amine protection in **9b** using BOC₂O. All new compounds and polymers have been characterized by ¹H and ¹³C NMR, mass spectrometry and so on. The data are consistent with the structures. Long chains (–OC₁₆H₃₃) were used on porphyrin to increase the solubility and indeed all porphyrin products are soluble in hexanes, CH₂Cl₂, THF and so on.

The GPC analyses indicate that **P1**, **P2**, **P3**, and **P4** are oligomers with degree of polymerization, DP, respectively of 7, 7, 11, and 6 (Table 1; GPC traces are in the Supporting

Table 1. GPC and TGA data of **P1**, **P2**, **P3**, and **P4**

	<i>M_n</i>	<i>M_w</i>	PD	DP	<i>T_{dec}</i> (deg)
P1	15400	28700	1.87	7	>300
P2	15400	21700	1.40	7	>300
P3	24400	39300	1.61	11	>300
P4	13200	21800	1.65	6	>270

Information). The fact that these materials are oligomers bringing about an interesting feature for this study. Indeed, the relative amount of terminal groups in comparison with the central units is large and consequently one can address the interactions (i.e., energy transfers) between these different chromophores. The thermal gravimetric analysis (TGA) recorded in the 25–810 °C range indicates decomposition at *T* > 250 °C in all cases, and even exceeding 300 °C from some cases (Table 1; GPC traces are in the Supporting Information). This thermal stability makes these materials appealing for applications. The first weight loss contributes to 50–68% of the total mass of the materials and occurs between ~250 and 500 °C. This weight loss is likely associated with the loss of the –OC₁₆H₃₃ chains accounting for ~62%.

During the course of this investigation, the potential intermediates **10a** and **10b** were prepared and were also used as model compounds for structural analysis purposes (Figure 1), namely in monitoring the dihedral angle formed by the average plane of the central α,α-quinone and maleimide with their peripheral benzene groups, θ and θ', as a function of the

position of their low energy charge transfer band, CT (Table 2).

For a more complete data set, these data are also compared to that of compounds **11** and **12** previously reported by us (Figure 1).^{10c} It is assumed that θ and θ' are weakly affected by the nature of the group X, so a three member series can adequately be compared. Indeed, the average θ and θ' and position of the CT band for **10a**, **12** and **10b** are respectively ~32, ~69, and ~86° and 386, 367, and 351 nm (X = I). Conclusively, as the planarity improved (i.e., θ and θ' decreases), the position of the CT band red-shifts as if the materials would behave as they were conjugated, although formally they are not. This conclusion strongly supports the findings previously stressed by us on other related polymers (containing the *trans*-Pt(PBu₃)₂ unit instead of [Zn]).^{10c} The averaged θ and θ' for **11** and **12**, respectively 69 and 60°, cannot account for the large difference in CT band positions (X = I), respectively at 382 and 367 nm. This is explained by the better electron acceptor ability of the α,α-quinone group (in **12**) vs that for maleimide (in **11**).^{10c} Finally, the red-shifts of the CT bands going from X = I to X = C≡CSiMe₃ is simply due to extension of the conjugated π-systems.

Electrochemistry. The cyclic voltammograms, CV, of **M1**, **M2**, **P1**, **P2**, **P3**, and **P4** are shown in Figure 2. Only chemically irreversible reduction waves are noted in the ~–1.8 to 0 V vs SCE range whereas the 0 to +1.3 V window is electrochemically silent (i.e., no oxidation wave attributable to the C≡C–[Zn]–C≡C unit was observed). On the basis of previous electrochemical studies, the reduction signal is associated with the reduction of the quinones and anthraquinones.^{6,8a,d} This conclusion is supported by DFT calculations below. For comparison purposes, the CV traces for **P4** exhibits the same peak potentials as for the polymer (C≡C–[Pt]–C≡C–AQ)_{*n*} (AQ = 2,2'-anthraquinone),⁶ suggesting that there is minimal effect between [Zn] and [Pt], except for the irreversibility in **P4**. The comparison with **M2** is also useful. The CV for **M2** (i.e., AQ–C≡C–[Zn]–C≡C–AQ) exhibits a reduction peak at –1.55 V with a weak shoulder at ~–1.35 V meaning that little modifications (nearly a shift of ~0.15 V) is observed. This is also consistent with the similar observation made for AQ–C≡C–[Pt]–C≡C–AQ.⁶ In the case of **M1** and **P2**, the reduction peak positions are expectedly not the same as the electron acceptors are different (quinone vs naphtha-quinone). The acceptor with the least conjugated π-bonds is indeed harder to reduce (i.e., quinone). Attempts to prepare the corresponding model compounds with quinones failed stubbornly as the unsubstituted side of the quinone proved reactive during the synthesis. The key result is that the first reduction waves are similar (i.e., –1.31, –1.36, –1.24, and –1.24 V vs SCE for **P1**, **P2**, **P3**, and **P4**, respectively) but should not necessarily be reflected by the position of the CT bands because of the irreversibility of the process.

Optical Properties. The characteristic absorption features (Figure 3) associated with the [Zn] chromophore are noted in the 400–500 nm range (Soret) and 500–650 nm for the Q-region (usually two bands for metalloporphyrins; see data in Table 3). Above 700 nm, a feature associated with a CT process is detected. This assignment is made based upon previous findings for **P5a** and **P5b** (Chart 1)^{8c} and DFT computations placed below. The exception in this list is **P3**, a polymer composed of the weakly accepting quinone maleimide, for which the spectral signature resembles more that of a metalloporphyrin alone⁴⁴ (i.e., typical ππ* signature at ~650 nm with

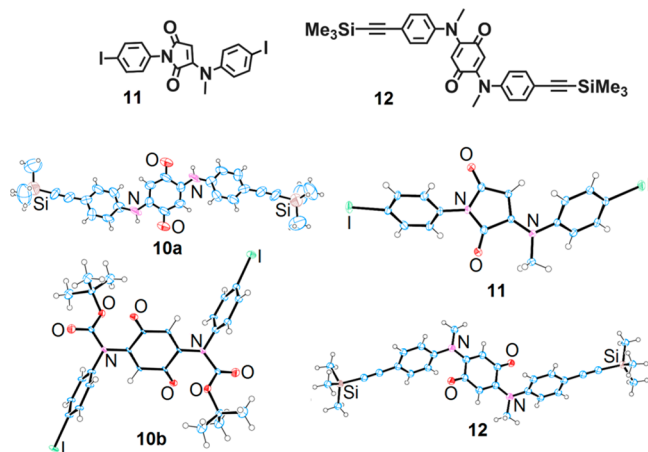
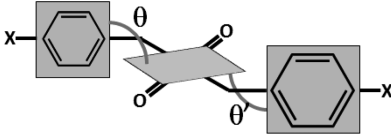


Figure 1. ORTEP drawings of **10a,b**, **11**,^{10c} and **12**.^{10c} The thermal ellipsoids are represented at 50% probability. Some details are provided in the Supporting Information for convenience.

Table 2. Dihedral Angles and CT Absorption Position of 10a and 10b, 11 and 12



	central plane	N–R	X	θ and θ' (deg)	$\lambda(\text{CT})$ (nm) in 2MeTHF at 298 K ^c
10a	α,α -quinone	N–H	C \equiv C–SiMe ₃	32.02 and 32.02	386 (X = I), 401 (X = C \equiv C–SiMe ₃) ^a
12 ^{10c}	α,α -quinone	N–Me	C \equiv C–SiMe ₃	65.80 and 72.41	367 (X = I), 370 (X = C \equiv C–SiMe ₃) ^a
10b	α,α -quinone	N–BOC	I	85.98 and 86.04 ^b 84.74 and 86.83 ^b	351 (X = I)
11 ^{10c}	maleimide	N–Me	I	55.48 and 64.55	382 (X = I)

^aIt is assumed that θ and θ' are weakly affected by the nature of the group X. ^bThere are two crystallographically independent molecules in the unit cell. ^cThere is another feature in the 500–600 nm range but the maximum cannot be accurately extracted (see Supporting Information for the spectra).

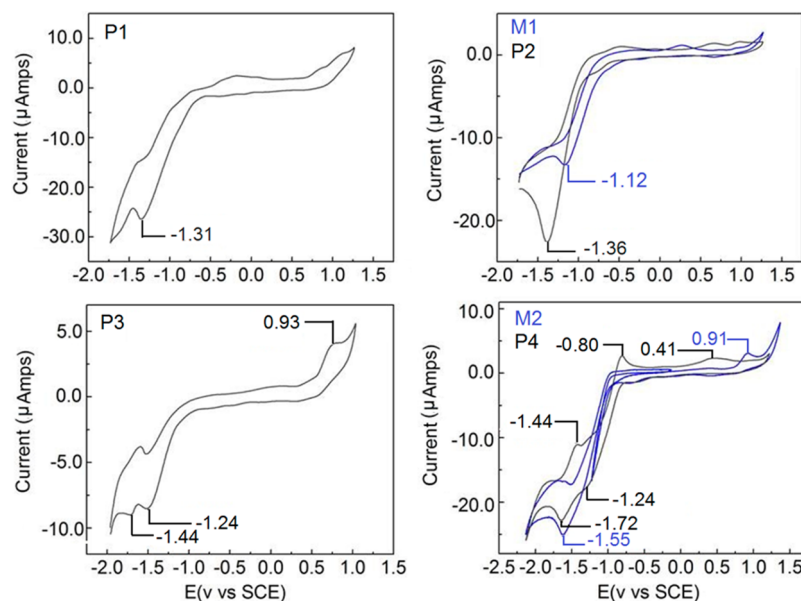


Figure 2. Cyclic voltammetry of M1, M2 (blue), P1, P2, P3, and P4 (both 4.0×10^{-3} M in THF with 0.1 M NBu₄PF₆). Scan rate = 50 mV/s.

no extra feature above 700 nm) suggesting that the porphyrine chromophore does not seemingly interact strongly with this quinone acceptor. Indeed, the DFT computations below corroborate this observation.

DFT and TDDFT Computations. The geometry of the M1 and M2 models were first optimized and the presentations of selected frontier MOs and relative contributions of the donor and acceptor fragments to these MOs are placed in Figure 5 and Table 4.

The atomic orbital contributions of the HOMO is mainly composed of the C \equiv C–[Zn]–C \equiv C π -system for both models with relative contributions of respectively 72 and 88%, the remainder being localized on the quinone π -systems. Conversely, the LUMO exhibits atomic orbital contributions located on the π -systems of the quinones (93 and 60% for M1 and M2, respectively). The remainder is located on the C \equiv C–[Zn]–C \equiv C π -system. The HOMO \rightarrow LUMO transitions are consistent with the expected CT processes C \equiv C–[Zn]–C \equiv C \rightarrow A. The 40/60% distribution for the C \equiv C–[Zn]–C \equiv C/anthraquinone fragments makes this CT process rather moderate compared to that for M1. TDDFT calculations (Table 4) place the pure electronic transitions at 793.5 and 701.3 nm for M1 and M2, respectively, which compare

reasonably with the experimental data (735 and 674 nm Table 3). The trend of the calculated oscillator strength is $f(\text{M2}) > f(\text{M1})$ and is also consistent with the observed absorptivity values, ϵ (i.e., $\epsilon(\text{M2}) > \epsilon(\text{M1})$, Table 2). A bar graph reporting f as a function of wavelength is shown in Figure 4 (bottom). By applying an arbitrary thickness of 1000 cm⁻¹ to each transition, a spectrum is generated. A qualitative resemblance between the calculated and experimental spectra is noted. The calculated upper energy transitions produced by HOMO and H – 1 \rightarrow L + 2 and L + 3 are reminiscent with the expected π,π^* features associated with the Q-bands placing these peaks in the region normally expected. These transitions also exhibit some modest mixing with CT contributions due to the presence of weak MO contributions of the acceptor quinone (see L + 2 for M2 as an example) or the presence of many individual transitions mixed together in which one of them is a CT process (see entry at 612.6 nm for M2).

The representation of selected frontier MOs for A–C \equiv C–[Zn]–C \equiv C–A–C \equiv C–[Zn]–C \equiv C–A used as models for P1–P4, their normalized distributions of the fragment orbital contributions, selected calculated positions of the pure electronic transitions, oscillator strengths (f), and their major contributions are provided in Figure 5 and Table 5,

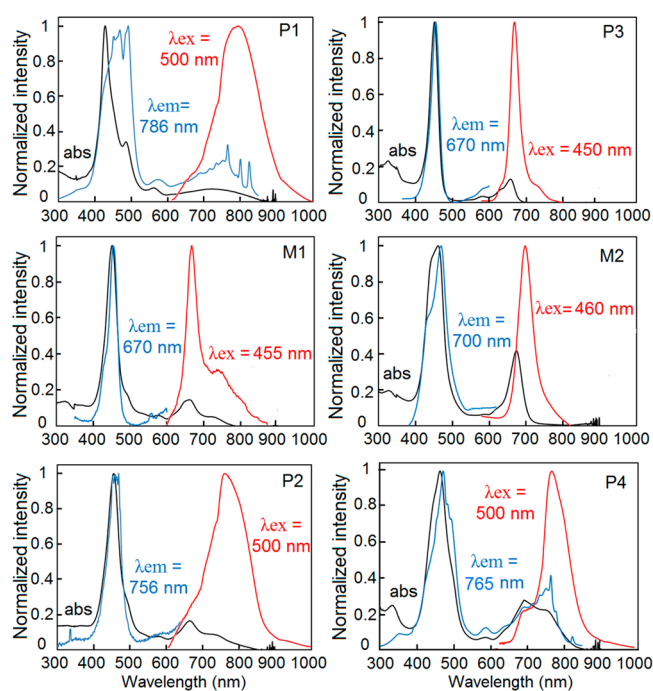


Figure 3. Absorption (black), excitation (blue) and fluorescence (red) spectra of **M1**, **M2**, **P1**, **P2**, **P3**, and **P4** in THF at 298 K.

Table 3. Absorption Data for $[\text{Zn}]$,⁴⁵ **M1**, **M2**, **P1**, **P2**, **P3**, and **P4**

	λ_{abs} (nm) (ϵ ($\text{M}^{-1} \text{cm}^{-1}$)), THF (298 K)
$[\text{Zn}]$	434 (282000), 444 (252000), 574 (21400), 622 (26200)
M1	454 (299000), 661 (59000), 735 (10400)
M2	440 (147300), 461 (161000), 674 (65000)
P1	430 (126000), 486 (67000), 562 (16000), 750 (17500)
P2	454 (196000), 665 (33000), 738 (17500)
P3	452 (243700), 658 (30300)
P4	461 (126000), 690 (34800), 755 (27500)

respectively. The C_6H_{13} groups have been replaced by CH_3 to minimize computer time.

The results can be divided into two groups: (1) **P1**, **P2**, and **P4** and (2) **P3**. The former group exhibits obvious CT processes in the same manner described for **M1** and **M2**, whereas the second one (**P3**) does not (see the top of Table 5 for a clear trend). The lack of CT processes in **P3** is fully consistent with the experimental data (Figure 3) where no CT feature normally detected >700 nm is noted. For the first group (**P1**, **P2**, and **P4**), the CT processes are obvious, both experimentally and computationally. Again, this list contains a fully conjugated system (isoindigo; **P1**), an unconjugated system but conjugated to the ketone (anthraquinone; **P4**), and a formally unconjugated system between the porphyrin chromophore and the quinone acceptor (α,α -quinone; **P2**). These computations place the CT peaks $\lambda(\text{P1}) > \lambda(\text{P2})$ as experimentally observed, whereas $\lambda(\text{P4})$ is calculated at a lower position but is observed at a higher wavelength of $\lambda(\text{P1})$ and $\lambda(\text{P2})$. As the position of the CT band is found sensitive to the dihedral angle made by the average quinone plane vs that of the flanking benzenes (up to 35 nm; Table 2), and it is not clear whether this angle is the same for the experimental and the computations (even in a THF solvent field). No reliable explanation is available for this discrepancy. Nevertheless, the

calculations corroborate well the presence of low-lying CT states.

Emission Properties. The **M1**, **M2**, **P1**, **P2**, **P3**, and **P4** in 2MeTHF are emissive at 298 K (Figure 3; see Table 6 for the photophysical parameters).

No obvious aggregation phenomenon was depicted in the 10^{-6} to 10^{-7} M concentration range used (see below). The excitation spectra superpose well the absorption indicating that the emitting species are the same as the absorbing ones (i.e., no signal from possible impurities). The emission bands turned out to be particularly large for **P1**, **P2**, and **P4** at 298 K. One reason stems from the presence of two emissions, a blue- and red-shifted ones arising respectively from the terminal and central units, commonly observed in oligomers.⁴⁶ This is particularly evident when comparing the spectra of **M1** with that for **P2** and **M2** with **P4** (Figure 3). Indeed, the emission of a low intensity shoulder on the blue side of the main band (at ~ 650 and ~ 700 nm for both **P2** and **P4**, respectively).

However, multiple emissions should not occur for monomeric models but it is seemingly the case for **M2**, which exhibits a strong narrow emission signal placed at higher energy than the low energy absorption. This observation is unusual but not without precedent for this class of compounds. Indeed for **P5a** and **P5b**, such a similar situation was observed where a fluorescence from the Q^- (weaker in this case) and CT bands (stronger) were noted.^{8c} The new feature in **M2** is that the high energy emission is inexplicably more intense than that of the S_1 CT luminescence. These two parameters, terminal and central chromophores, and the possibility of two states emitting from a same chromophore, indicate that these emissions are likely to exhibit multiple components. This is indeed the case (Table 6). In all cases, the lifetimes are in the ps or short ns time scales indicating that the emissions are fluorescence. This observation is also consistent with the strong spectral overlaps between the emission and absorption (i.e., small Stokes shifts). Two components are readily depicted in the time-resolved spectra where the high and low energy bands are short- and long-lived, respectively.

The **M1** and **M2** models bare only one $\text{C}_6\text{H}_4\text{C}\equiv\text{C}-[\text{Zn}]-\text{C}\equiv\text{CC}_6\text{H}_4$ unit and their dual emissions are unambiguously not related to terminal vs central units (Figure 6). For comparison purposes, the reported absorption (669 nm) and fluorescence (678 nm) 0–0 peaks and fluorescence lifetime, τ_F (2.04 ns), for $\text{Me}_2\text{NC}_6\text{H}_4\text{C}\equiv\text{C}-[\text{Zn}]-\text{C}\equiv\text{CC}_6\text{H}_4\text{NMe}_2$ (with di-*ortho*-substituted aryls at the *meso*-positions) in THF, are considered.⁴⁷ On this basis, the fluorescence position at 690 nm for **M1** is strongly reminiscent of the $\text{S}_1 \pi\pi^*$ for this chromophore and the longer wavelength band at 760 nm is an emission arising from the CT state. Unsurprisingly, the ultrafast τ_F for the high energy fluorescence (7.7 ps) is associated with a very efficient nonradiative relaxation down to the S_1 CT state. The latter state also emits with an ultrafast kinetic (~ 35 ps).

M2 exhibits two very closely located fluorescence bands (645 and 665 nm) and cannot be respectively attributed to $\text{S}_1 \pi\pi^*$ and CT emissions as this was the case for **M1**. The lowest energy excited state in **M2** is a moderate CT state (significantly mixed with $\pi\pi^*$ contribution of $\text{C}\equiv\text{C}-[\text{Zn}]-\text{C}\equiv\text{C}$ unit; see DFT results in Table 4). In fact, **M2** can exist as *cis*- and *trans*-isomers as previously demonstrated for an anthraquinone- $[\text{Pt}]$ -anthraquinone compound readily detected by ^{31}P NMR in this case.⁶ Unfortunately, these isomers in **M2** could not be neither confirmed by ^1H or ^{13}C NMR nor separated by column

Table 4. (Top) Distributions of the Normalized Fragment Orbital Contributions of the Frontier MO's for M1 and M2, Where the Major Contributions are in Bold, and (Bottom) Selected Calculated Positions of the Pure Electronic Transitions, Oscillator Strengths (f), and Major Contributions.^a

M1	H - 4	H - 3	H - 2	H - 1	H	L	L + 1	L + 2	L + 3	L + 4
C≡C-[Zn]-C≡C	1.00	0.39	0.19	1.00	0.72	0.07	0.01	0.80	1.00	0.52
benzene- <i>N</i> -naphthoquinone	0.00	0.61	0.81	0.00	0.28	0.93	0.99	0.20	0.00	0.48
M2	H - 4	H - 3	H - 2	H - 1	H	L	L + 1	L + 2	L + 3	L + 4
C≡C-[Zn]-C≡C	0.76	0.99	0.99	1.00	0.88	0.40	0.05	0.48	1.00	0.19
anthraquinone	0.24	0.01	0.01	~ 0.0	0.12	0.60	0.95	0.52	~ 0.0	0.81
λ (nm)	F major contributions (%) for M1									
793.5	0.7098 HOMO \rightarrow LUMO (97)									
768.0	0.0000 HOMO \rightarrow L + 1 (98)									
638.1	0.8064 HOMO \rightarrow L + 2 (90)									
610.5	0.0053 H - 1 \rightarrow LUMO (32), H - 1 \rightarrow L + 2 (18), HOMO \rightarrow L + 3 (50)									
571.5	0.0000 H - 1 \rightarrow L + 1 (99)									
λ (nm)	F major contributions (%) for M2									
701.3	1.2960 HOMO \rightarrow LUMO (96)									
622.9	0.0000 HOMO \rightarrow L + 1 (99)									
612.6	0.0161 H - 1 \rightarrow LUMO (71), HOMO \rightarrow L + 3 (27)									
563.6	0.0257 H - 1 \rightarrow L + 3 (12), HOMO \rightarrow L + 2 (87)									
538.5	0.0000 H - 1 \rightarrow L + 1 (100)									
521.1	0.0812 H - 1 \rightarrow LUMO (22), H - 1 \rightarrow L + 2 (46), HOMO \rightarrow L + 3 (32)									

^aThe 100th transitions are placed in the Supporting Information.

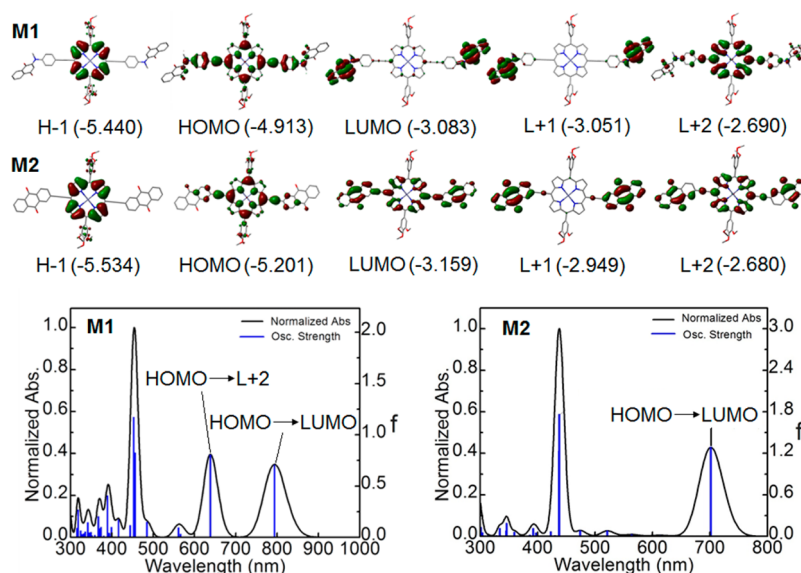


Figure 4. Top: selected MOs for M1 and M2 (H = HOMO, L = LUMO; energy in eV; see Supporting Information for H - 4 to L + 4). Bottom: bar graph (blue) reporting their electronic transition positions vs f (oscillator strength). The black line is a spectrum where 1000 cm^{-1} is applied to each transition. The CH_3 groups are used to minimize calculation times.

chromatography. The τ_F values of P4 (77 and 765 ps) are in the same order of magnitude (109 and 708 ps) but could not be specifically assigned. The time-resolved fluorescence spectra of the polymers exhibit dual components as well (Figure 7), but their origins differ from the models.

For the formally unconjugated P3 polymer, the nature of the S_1 excited state is again a $\pi\pi^*$ state localized in the $\text{C}\equiv\text{C}-[\text{Zn}]-\text{C}\equiv\text{C}$ chromophore (Table 5). The time-resolved spectra exhibit two species with narrow peaks at 640 ($\tau_F = 680 \text{ ps}$) and 645 nm ($\tau_F = 2.5 \text{ ns}$). These species are easily identified as the less extended π -conjugated terminal ($\text{C}\equiv\text{C}-[\text{Zn}]-\text{Br}$) and the more π -conjugated central ($\text{C}\equiv\text{C}-[\text{Zn}]-\text{C}\equiv\text{C}$) groups, which stem from the reaction $6 + 7 \rightarrow \text{P3}$ in

1:1 stoichiometry (Scheme 1). The shorter τ_F (680 ps) is most likely due to the expected heavy atom effect (i.e., Br), although the commonly encountered S_1 energy transfer (terminal* \rightarrow central)^{46,48} is strongly considered. In such a case, the rate for energy transfer, k_{ET} is given by $k_{\text{ET}} = (1/\tau_F) - (1/\tau_{F^*})$ where τ_F and τ_{F^*} are the fluorescence lifetime of the energy donor in the presence (here terminal) and absence of an energy acceptor (central unit is appropriate).⁴⁹ Then, $k_{\text{ET}} \sim 1.1 \times 10^9 \text{ s}^{-1}$. Such a rate is typical for multiporphyrin assemblies.⁵⁰

The time-resolved fluorescence spectra for P1, P2, and P4 are expectedly broad as deduced from Figure 3, well extending in the near-IR region. The τ_F values vary from 77 to 765 ps, a range similar to that found in the model compounds. Because

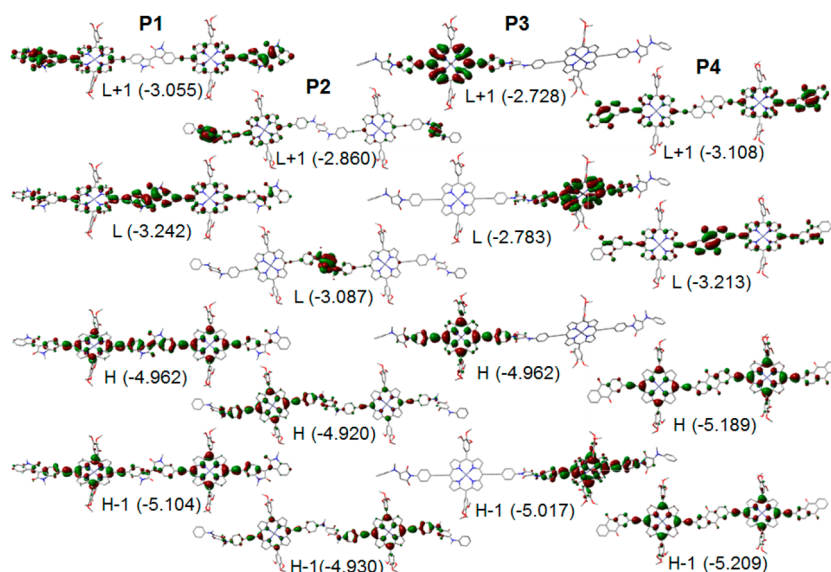


Figure 5. Selected MOs for A-C≡C-[Zn]-C≡C-A-C≡C-[Zn]-C≡C-A models for P1, P2, P3, and P4 (optimized geometry by DFT; H = HOMO, L = LUMO; energy in eV; see Supporting Information for H - 4 to L + 4).

Table 5. (Top) Normalized Distributions of the Fragment Orbital Contributions of the Frontier MO's for P1, P2, P3 and P4, Where the Major Contributions are in Bold, and (Bottom) Selected Calculated Positions of the Pure Electronic Transitions, Oscillator Strengths (f), and Major Contributions.^a

	H - 4	H - 3	H - 2	H - 1	H	L	L + 1	L + 2	L + 3	L + 4
P1										
C≡C-[Zn]-C≡C	0.21	1.00	1.00	0.77	0.73	0.38	0.34	0.10	0.62	0.59
isoindigo	0.79	0.00	0.00	0.23	0.27	0.62	0.66	0.90	0.38	0.41
P2										
C≡C-[Zn]-C≡C	0.13	1.00	1.00	0.73	0.71	0.09	0.27	0.19	0.57	0.62
α,α -quinone	0.87	0.00	0.00	0.27	0.29	0.91	0.73	0.81	0.43	0.38
P3										
C≡C-[Zn]-C≡C	0.23	1.00	1.00	0.83	0.82	0.86	0.88	1.00	1.00	0.04
maleimide	0.77	0.00	0.00	0.17	0.18	0.14	0.12	0.00	0.00	0.96
P4										
C≡C-[Zn]-C≡C	1.00	1.00	1.00	0.89	0.87	0.36	0.43	0.07	0.45	0.56
anthraquinone	0.00	0.02	0.02	0.11	0.13	0.64	0.57	0.93	0.55	0.44
	λ (nm)			F	major contributions (%) ^b					
P1	866.1			4.284	HOMO \rightarrow LUMO (93)					
	746.1			0.0095	H - 1 \rightarrow LUMO (83), HOMO \rightarrow L + 1 (14)					
P2	785.7			1.3331	H - 1 \rightarrow LUMO (85), HOMO \rightarrow LUMO (10)					
	773.6			0.0136	H - 1 \rightarrow LUMO (10), HOMO \rightarrow LUMO (86)					
P3	644.1			2.3127	H - 1 \rightarrow LUMO (51), HOMO \rightarrow L + 1 (38)					
	635.5			0.0901	H - 1 \rightarrow LUMO (35), HOMO \rightarrow L + 1 (51)					
P4	724.6			2.4902	H - 1 \rightarrow LUMO (82), HOMO \rightarrow L + 1 (14)					
	706.2			0.0021	HOMO \rightarrow LUMO (91)					

^aThe 100th transitions are placed in the Supporting Information. ^bThe bar graph reporting the position of the electronic transitions vs the oscillator strength (f) and line representing a spectrum where 1000 cm^{-1} is applied to each transition, are placed in the Supporting Information.

the fluorescence maxima of most components are $>700\text{ nm}$ (i.e., more red-shifted than the 0-0 peak of the Q-band), it is easy to deduce that the nature of these emissive states is CT. Consequently, their origin is again the shorter-lived terminal unit, which is generally blue-shifted, and central units (generally red-shifted), with P2 being the exception where both bands lie nearly on top of each other. Using the same approach mentioned above, the k_{ET} values extracted for P1, P2, and P4 are respectively $\sim 7.1 \times 10^9$, $\sim 12 \times 10^9$, and $4.5 \times 10^9\text{ s}^{-1}$. The overall fluorescence intensity is modest but typical for the [Zn] chromophore (see [tetra(meso-aryl)porphyrinato]zinc(II),

ZnTPP, for example, $\Phi_{\text{F}} = 0.03$; $\tau_{\text{F}} = 2.8\text{ ns}$).¹⁷ However, no phosphorescence was observed at all. The fs transient absorption spectroscopy was used to shine light on this phenomenon.

Femtosecond Transient Absorption Spectroscopy.

Prior to present the transient data, one comment is needed. The use of quinone⁵¹ and anthraquinone⁵² covalently attached to a porphyrin macrocycle is well documented in the literature where photoinduced electron transfers are reported and supported by various techniques. In all these literature cases, the linkage between the electron donor and acceptor is clearly

Table 6. Fluorescence Parameters and Closest Lifetime Components in the Transient Absorption Spectra at 298 K

	Φ_F ($\pm 10\%$) ^a	λ_{\max} (± 10 nm) ($\lambda_{\text{exc}} = 400$ nm)	τ_F (ps)	closest lifetime component in the transient absorption spectra (ps)
M1	0.013	690	7.7 ± 0.1	7.85 ± 0.02
		760	35.3 ± 0.2	
M2	0.051	645	109 ± 1	
		665	708 ± 1	636 ± 3
P1	0.014	755 (broad)	119 ± 1	
P2	0.005	780	750 ± 2	592 ± 5
		750 (very broad)	77 ± 1	47 ± 1
P3	0.033	750 (very broad)	765 ± 4	
		640	680 ± 20	366 ± 2
P4	0.012	645	2500 ± 600	
		740	166 ± 1	
		765	688 ± 2	474 ± 6

^aWith respect to H₂TPP ($\Phi_F = 0.11$) in ref 17.

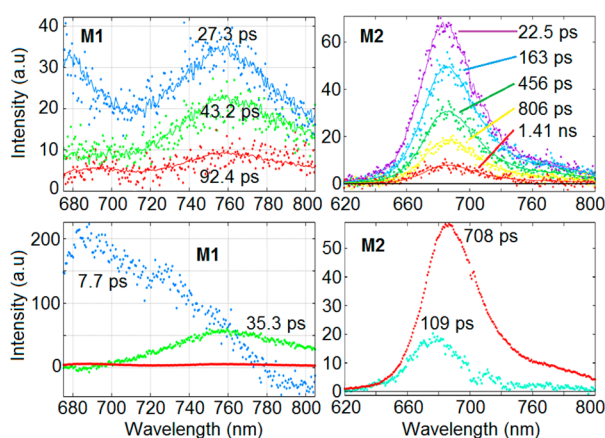


Figure 6. Top: time-resolved fluorescence spectra of M1 and M2 in THF at 298 K. Bottom: spectra of the different components with their lifetimes (Table 6) describing the spectral evolution. The component in red for M1 is a component providing a better fit. Note, the fluorescence intensity is not corrected for the detector response.

unconjugated or exhibits a drastic torsion angle preventing efficient conjugation. More diagnostic, in these reported spectra, no band exceeding 650 nm was observed (i.e., no CT band). On the basis of the DFT computations above, as the CT excited state already exhibits significant electronic density on the acceptor moieties (here quinone (P2) and anthraquinone (P4); see Table 5), then photoinduced electron transfer from the excited porphyrin to quinone and anthraquinone is clearly unlikely. Furthermore, no oxidation wave attributable to $\text{C}\equiv\text{C}-[\text{Zn}]-\text{C}\equiv\text{C}$ within the 0 to +1.4 V SCE window was detected. This observation suggests that oxidation of this unit must occur at a more positive potential (i.e., >+1.4 V) and consequently, the photoinduced electron transfer is indeed likely to be thermodynamically unfavorable.

The fs transient absorption spectra are provided in Figures 8 (M1 and M2) and 9 (P1–P4). Using $\lambda_{\text{exc}} = 650$ nm, the position of the 0–0 Q-band, the $S_n \pi\pi^*$ porphyrin manifold is populated allowing to monitor its relaxation kinetics along with those of the states in the vicinity including the T_n states, which expected to be low-lying (see DFT computations below). The positive and negative signals are respectively the bleach and the

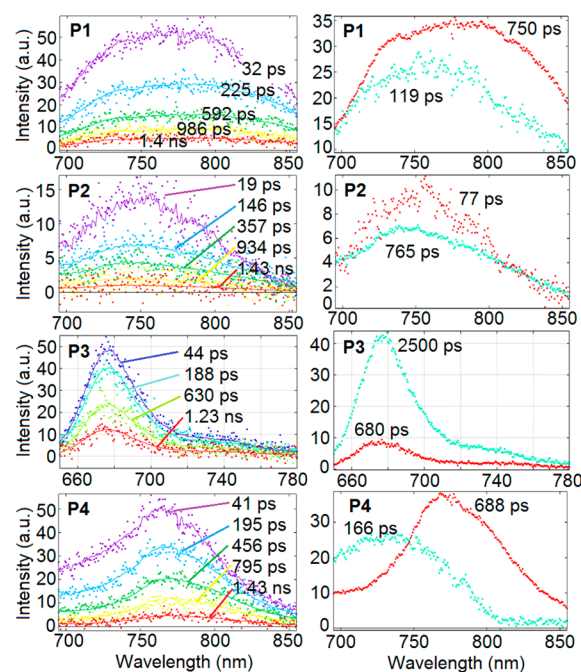


Figure 7. Left: Time-resolved fluorescence spectra of P1, P2, P3, and P4 in THF at 298 K. Right: spectra of the different components with their decay times (reported in Table 6) describing the spectra on the left. Note, the fluorescence intensity is not corrected for the detector response.

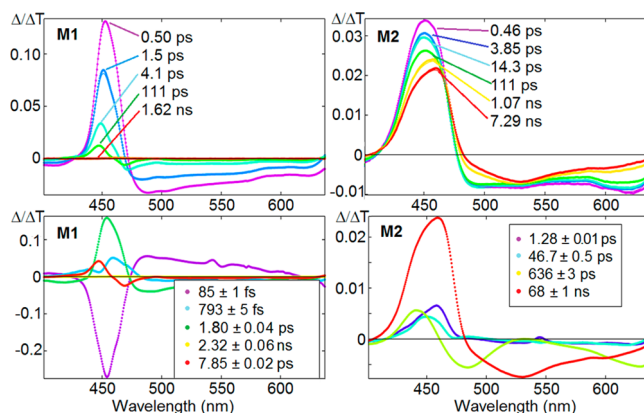


Figure 8. Top: Time evolution of the transient absorption spectra of M1 and M2 in 2MeTHF at 298 K, $\lambda_{\text{exc}} = 650$ nm, pulse width = 81 and 127 fs, respectively. Bottom: individual components describing the time evolution. Note that the components >8.6 ns are not accurate because of the limitation of the delay line.

transient bands. The evolution of the transient spectra was monitored from ~ 0 fs to 8.6 ns (limit of the delay line). These spectra were deconvoluted to extract each component along with their relaxation lifetimes (Table 7). The results turned out to be rather complex but particularly informative. The complexity is amplified by the well-known solvent-induced vibrational relaxation of the S_1 population containing the ZnTPP chromophore which occurs in the picosecond to tens of picoseconds range.⁵³ Such interactions lead to nonemitting species, and an extra component is expected for S_n species in the transient spectra.

First, any species with lifetimes larger than their corresponding fluorescence lifetimes extracted from the Streak camera data are unquestionably T_1 species ($T_1 \sim > S_0$). These lifetimes are

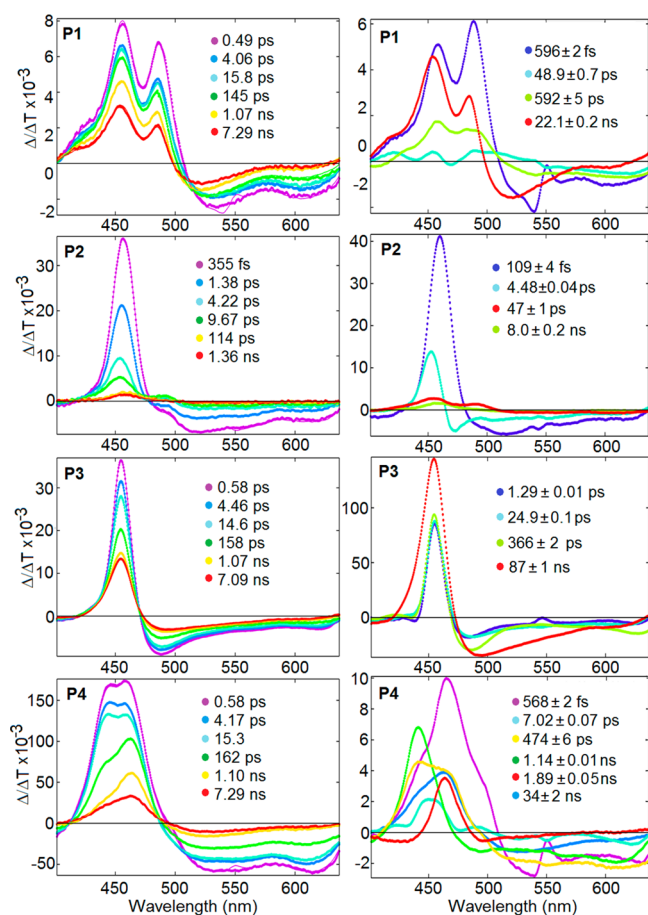


Figure 9. Left: Time evolution of the transient absorption spectra of P1–P4 in degassed solution of 2MeTHF at 298 K, $\lambda_{\text{exc}} = 650$ nm, pulse width = 127, 153, 115, and 143 fs, respectively. Right: individual components describing the time evolution. Note that the components > 8.6 ns are not accurate because of the limitation of the delay line.

Table 7. Transient Absorption Lifetimes (solvent = 2MeTHF)

	ultrafast components (fs)	other components (ps)	closest components to τ_{F} 's (ps)	triplet components (ns)
M1	85 ± 1 , 793 ± 5	1.80 ± 0.04	7.85 ± 0.02	2.32 ± 0.06
M2	1280 ± 10	46.7 ± 0.5	636 ± 3	68 ± 1
P1	596 ± 5	48.9 ± 0.7	592 ± 5	22.1 ± 0.2
P2	109 ± 4	4.48 ± 0.04	47 ± 1	8.0 ± 0.2
P3	1290 ± 10	24.9 ± 0.01	366 ± 2	87 ± 1
P4	568 ± 2	7.02 ± 0.07	474 ± 6	34 ± 2 1.14 ± 0.01 , 1.89 ± 0.05

2.32 ± 0.06 (M1), 68 ± 1 (M2), 22.1 ± 0.2 (P1), 8.0 ± 0.2 (P2), 87 ± 1 (P3) and 34 ± 2 ns (and maybe 1.89 ± 0.05 and 1.14 ± 0.01 ns) (P4). Qualitatively based on data of Tables 6 and 7, the short triplet lifetimes are also often associated with short τ_{F} and *vice versa*. Noteworthy, these triplet lifetimes are particularly fast in comparison with those reported for common porphyrin free bases and metalloporphyrins (generally ms).⁵⁰ This result explains well why no phosphorescence has been observed for all materials investigated. Although two components were depicted in the fluorescence spectra associated with terminal and central units, only one component

is noted for the triplet species (note that two other components at 1.89 ± 0.05 and 1.14 ± 0.01 ns are observed but their identity is uncertain). This result indicates that the nonradiative relaxation $T_n \gtrsim T_1$ and $T_n \gtrsim S_0$ are also very fast.

The best fits provide four to six components (P4 has six). After identifying the triplet species, the remainders are the singlet ones, which relax from 85 fs to several hundreds of ps. In many cases, it was possible to “match” the closest transient lifetime component with a fluorescence one (Table 6), hence helping the identification. The nonexact “match” stems from the large number of components needed to describe the transient data, and the lower intensity and the biexponential nature of the fluorescence. The shortest components range from ~ 0.09 to 1.29 ps (M1, 0.09 and 0.79; M2, 1.28; P1, 0.60; P2, 0.11, P3, 1.29; P4, 0.57 ps) and are reasonably assigned to S_n (most likely S_2 in this work) species (excited in the 0–0 peak of the Q-band), which rapidly relax to S_1 ($S_n \sim > S_1(\text{CT})$) or T_n ($T_n \sim > T_1(\text{CT})$), where this latter assignment for $T_1(\text{CT})$ is based on DFT computations provided below). Figure 10

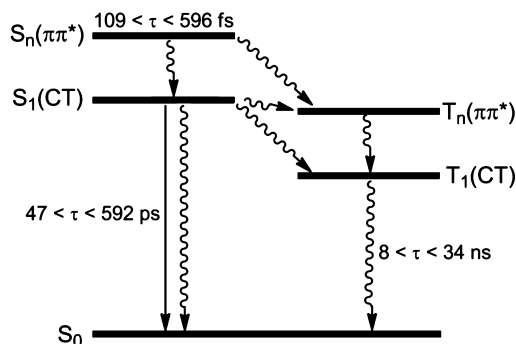


Figure 10. Energy diagram for P1, P2, and P4 along with their deactivation time scales. In this diagram, the manifold associated with terminal and central units are neglected for sake of simplicity. Note that the position of the T_n manifold is not known and that the straight arrow is fluorescence and the wave arrows indicate nonradiative processes.

summarizes the energy diagram and the transient lifetimes applied to the push–pull polymers P1, P2 and P3. Finally, the last components, listed as M1, 1.8; M2, 46.7; P1, 48.9; P2, 4.5; P3, 24.9; and P4, 7.0 ps, are likely solvent-induced vibrational relaxation of the S_n population containing the $\text{C}\equiv\text{C}-[\text{Zn}]-\text{C}\equiv\text{C}$ chromophore as the time scale is consistent with those reported for ZnTTP.⁵³

The key conclusion of the fs transient absorption measurements is that the low fluorescence intensity and absence of phosphorescence are mostly due to the particularly fast nonradiative deactivation kinetics (mostly ~ 100 fs to several hundred of ps). The relaxation of the triplet species ($T_1 \sim > S_0$; $2 < T_1 < 87$ ns) is a clear evidence for this phenomenon.

Aggregation of the Polymers and Solid State. The absorption and emission spectra of P2 and P4 were investigated in the solid state (Figure 11) and both series exhibit broad and significantly red-shifted signals with respect to solution. In order to shine light on this phenomenon, the polymers were investigated in solution at 298 and 77 K for three concentrations (10^{-4} , 10^{-5} and 10^{-6} M, in 2MeTHF; for comparison of all materials see Supporting Information).

At lower concentrations, the fluorescence bands are blue-shifted and of medium intensity. This lower intensity is expected from the lower optical density. Upon increasing the

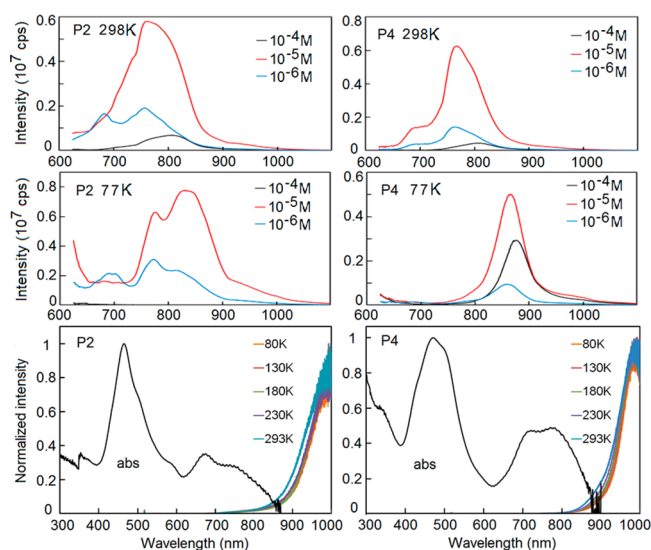


Figure 11. Fluorescence spectra of **P2** and **P4** in 2MeTHF at 298 (top) and 77 K (middle) as a function of concentration. Bottom; absorption (black) at 298 K and emission (various colors) spectra as a function of temperature of **P2** and **P4** in the solid state. The emission intensity has been normalized for convenience.

concentration (10^{-5} M), the intensity increases but new features start appearing on the red side of the spectrum (see **P2** and **P4** for a notable examples). Upon further increase of the concentration (10^{-4} M), the shifting of the fluorescence band to the red side continues but the intensity decreases also. This decrease is due a combination of an optical density issue (too opaque for the incident and emitted light to go through the sample) and lower quantum efficiencies in the high concentration state. The second effect is easily verified from the expected decrease in emission lifetimes (as demonstrated below for **P1–P4**). The red-shifting upon cooling and increasing the concentration is typical for an aggregation phenomenon.⁵⁴ In the solid state, both **P2** and **P4** exhibit maxima around 980 nm and the total intensity increases upon cooling from 298 to 80 K. The normalization of the spectra allows for the detection of a small variation of the intensity at 900 nm. The polymers have been investigated at 77 K where aggregation takes place (Figure 12 and Table 8). Again, the maxima have shifted to the red and the time-resolved spectra also indicate shorter multiple components (at least 2 or 3).

For the polymers, the τ_F data are systematically shorter, which is consistent with the observed decrease in fluorescence intensity upon aggregation. For comparison purposes the model compounds **M1** and **M2** were investigated as well. The concentration and temperature effects on the spectra (band shapes and positions) are more modest (see Supporting Information). The τ_F data for **M1** increase drastically whereas those for **M2** remains within the same order of magnitude. It is concluded that aggregation is possible for these monoporphyrim units but the larger size of the polymers in comparison with the model compounds leads to more nonradiative deactivation pathways.

Triplet state. The measurements of the fluorescence lifetimes of all materials in solution provided no evidence for long components suggesting the presence of phosphorescence. DFT was used to predict their positions by calculating the difference between the total energy of the ground and lowest energy triplet excited states (Table 9). Moreover the nature of

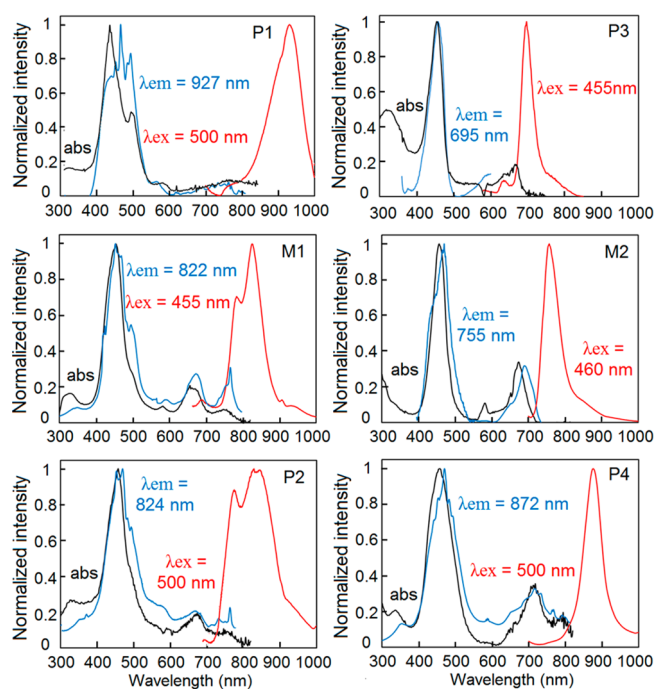


Figure 12. Absorption (black), excitation (blue), and fluorescence (red) spectra of **M1**, **M2**, and **P1–P4** in 2MeTHF at 77 K.

Table 8. Emission Wavelength and Lifetimes at 77 K (i.e. aggregation state)

	λ_{abs} (nm), 2MeTHF	λ_{max} (± 5 nm) ^a	τ_F (ps)
M1	452, 658, 744	785	114 \pm 1
		830	577 \pm 1
M2	454, 584, 672	735	19.8 \pm 0.3
		755	101 \pm 1
		770	647 \pm 5
P1	430, 485, 755	810 (very broad)	13.9 \pm 0.4
		860	74 \pm 1
P2	456, 668, 750	770 (broad)	15.4 \pm 0.4
		840	67.4 \pm 0.9
P3	452, 664	690	181 \pm 1
		700	53.5 \pm 0.5
		700	820 \pm 4
P4	454, 706, 786	820	10.5 \pm 0.4
		860	47.9 \pm 0.5
		875	201 \pm 2

^aThe time-resolved fluorescence at 77 K spectra are placed in the Supporting Information.

the lowest and highest semioccupied molecular orbitals (LSOMO and HSOMO, respectively) has also been addressed (Figure 13).

The description of the triplet state T_1 can be reasonably made on the basis of the atomic contributions of the LSOMO and HSOMO. Assuming that the MOs generating the S_1 state, which are mainly HOMO and LUMO based on the data in Table 5, then it is reasonably expected a similarity between LSOMO and HOMO and HSOMO and LUMO. Indeed, the calculated LSOMO and HSOMO representations are reminiscent to those corresponding HOMO and LUMO, respectively.

Table 9. Predicted Position (from DFT Computations) of the Phosphorescence 0-0 Peaks

compound	T_1-S_0 energy gap		calculated $T_1 \rightarrow S_0$ wavelength (nm)
	hartree	eV	
P1 model	0.033 13	0.90	1378
M1	0.044 10	1.20	1033
P2 model	0.035 11	0.96	1292
P3 model	0.045 95	1.25	992
M2	0.044 82	1.22	1016
P4 model	0.044 77	1.22	1016

CONCLUSION

Four new push–pull polymers of the general formula $(C\equiv C-[Zn]-C\equiv C-A)_n$, all exhibiting a S_1 CT excited state at various extents with very different structural features, notably a fully conjugated polymer (P1), a formally nonconjugated but exhibit strong electronic communication across the chain (P2), a formally nonconjugated material but local conjugation between the donor and acceptor occurs (P4), and one bearing a weak acceptor and used for comparison (P3), have been reported. The three former polymers are near-IR emitters with $\lambda_{max} > 750$ nm. These polymers appear as oligomers providing the opportunity to investigate the photophysical properties of the terminal unit as they act as antenna to the central core of the polymer chain, thus exhibiting a dual fluorescence arising from the terminal to the central units. Both, the emission intensities and lifetimes are respectively weak and short-lived, smaller than what is expected for the common ZnTPP. The fluorescence and fs transient absorption spectra kinetics indicate that the $S_1(CT)$ (from 77 to 765 ps; fluorescence decays and from 47 to 592 ps; transient absorption) and the nonemissive $T_1(CT)$ (from 8 to 34 ns; transient absorption) states are very short-lived for P1, P2 and P4. The same polymers excited within the 0–0 peak of the Q-band (650 nm) also relax nonradiatively rather quickly (from 109 to 596 fs; i.e., $S_n(\pi\pi^*) \sim > S_1(CT)$ and $S_n(\pi\pi^*) \sim > T_n(\pi\pi^*)$, $T_1(CT)$). When the concentration is increased or the solution is cooled, new red-shifted bands appear in the spectra, which witness the presence of an aggregation phenomenon. The overall fluorescence intensity

decreases as well as the fluorescence lifetimes. In the solid state, the emission maximum shift all the way to 980 nm, representing a red-shift of more than 200 nm in comparison with the maxima observed in solution at 298 K under dilute conditions. Finally, DFT computations predict that the T_1 manifold should be found between 1000 and 1400 nm.

All in all, the investigation of these push–pull polymers indicates the presence of rather complex processes, which in these cases, are ultrafast. The next question is within the bulk heterojunction solar cells built upon push–pull conjugated polymers such as those or others, are the rates for the migration of the excitation energy (from the center of the bulk to the interface with the electron acceptor; often PCBM, phenyl- C_{61} -butyric acid methyl ester) and the excited state lifetimes of the electron donors within the polymers long enough to efficiently inject electrons into the PCBM-containing phase? This work indirectly demonstrates that these kinetic parameters must clearly play in the magnitude of the solar cell efficiency.

ASSOCIATED CONTENT

Supporting Information

The Supporting Information is available free of charge via the Internet at The Supporting Information is available free of charge on the ACS Publications website at DOI: 10.1021/acs.macromol.5b01607.

X-ray data, TGA and GPC traces, UV–vis spectra of 3, 9b, 10a, 10b, 11, and 12 in THF at 298 K, DFT and TDDFT computation results, time-resolved fluorescence spectra at 77 K, and 1H and ^{13}C NMR spectra of the compounds and polymers (PDF)

AUTHOR INFORMATION

Corresponding Author

*(P.D.H.) E-mail: Pierre.Harvey@USherbrooke.ca.

Notes

The authors declare no competing financial interest.

ACKNOWLEDGMENTS

This research was supported by the Natural Sciences and Engineering Research Council of Canada (NSERC), the Centre

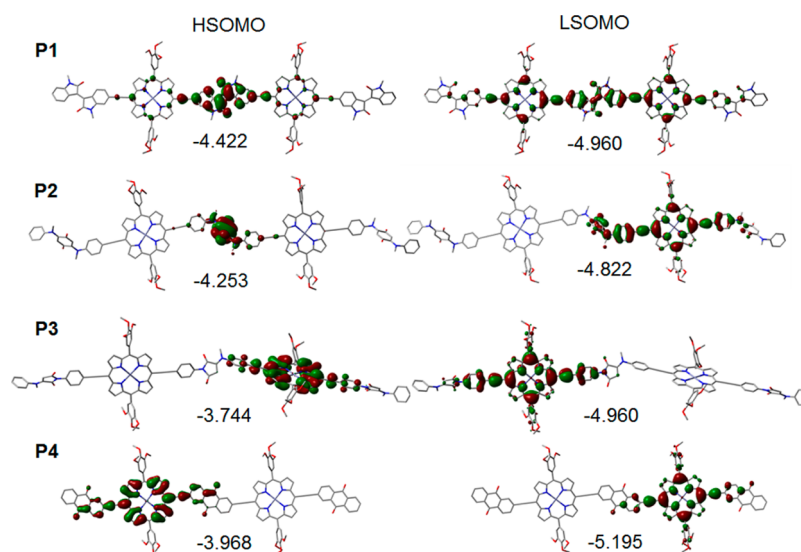


Figure 13. MO representations of LUMO and HOMO for P1, P2, P3, and P4. See Supporting Information for M1 and M2.

Québécois des Matériaux Fonctionnels (CQMF), and the Centre d'Études des Matériaux Optiques et Photoniques de l'Université de Sherbrooke (CEMOPUS). X.W. thanks the China Scholarship Council for a scholarship. Prof. Christian Reber and M. Pierre Libioule, Université de Montréal, are thanked for the measurements of the solid state emission spectra of P2 and P4.

REFERENCES

- (1) (a) Jemison, R. C.; McCullough, R. D. *ACS Symp. Ser.* **2014**, *1161*, 71–109. (b) Pron, A.; Berrouard, P.; Leclerc, M. *Macromol. Chem. Phys.* **2013**, *214*, 7–16. (c) Duan, C.; Huang, F.; Cao, Y. *J. Mater. Chem.* **2012**, *22*, 10416–10434. (d) Kulhánek, J.; Bureš, F. *Beilstein J. Org. Chem.* **2012**, *8*, 25–49. (e) Liao, R.; Liu, C.; Sa, R.; Wu, K. *J. Mol. Struct.: THEOCHEM* **2007**, *823*, 28–33. (f) Roncali, J.; Blanchard, P.; Frere, P. *J. Mater. Chem.* **2005**, *15*, 1589–1610. (g) Kesters, J.; Verstappen, P.; Kelchtermans, M.; Lutsen, L.; Vanderzande, D.; Maes, W. *Adv. Energy Mater.* **2015**, DOI: 10.1002/aenm.201500218.
- (2) (a) Zhou, W.; Jin, F.; Huang, X.; Duan, X. M.; Zhan, X. *Macromolecules* **2012**, *45*, 7823–7828. (b) Sprafke, J. K.; Kondratuk, D. V.; Wykes, M.; Thompson, A. L.; Hoffmann, M.; Drevinskas, R.; Chen, W.-H.; Yong, C. K.; Kärnbratt, J.; Bullock, J. E.; Malfois, M.; Wasielewski, M. R.; Albinsson, B.; Herz, L. M.; Zigmantas, D.; Beljonne, D.; Anderson, H. L. *J. Am. Chem. Soc.* **2011**, *133*, 17262–17273. (c) Huang, X.; Shi, Q.; Chen, W.-Q.; Zhu, C.; Zhou, W.; Zhao, Z.; Duan, X.-M.; Zhan, X. *Macromolecules* **2010**, *43*, 9620–9626. (d) Huang, X.; Zhu, C.; Zhang, S.; Li, W.; Guo, Y.; Zhan, X.; Liu, Y.; Bo, Z. *Macromolecules* **2008**, *41*, 6895–6902. (e) Zhang, L.; Wang, K.; Qian, X.; Liu, H.; Shi, Z. *ACS Appl. Mater. Interfaces* **2013**, *5*, 2761–2766. (f) Duncan, T. V.; Susumu, K.; Sinks, L. E.; Therien, M. J. *J. Am. Chem. Soc.* **2006**, *128*, 9000–9001. (g) Fenwick, O.; Sprafke, J. K.; Binias, J.; Kondratuk, D. V.; Di Stasio, F.; Anderson, H. L.; Cacialli, F. *Nano Lett.* **2011**, *11*, 2451–2456. (h) Wang, L.; Shi, S.; Ma, D.; Chen, S.; Gao, C.; Wang, M.; Shi, K.; Li, Y.; Li, X.; Wang, H. *Macromolecules* **2015**, *48*, 287–296. (i) Umeyama, T.; Takamatsu, T.; Tezuka, N.; Matano, Y.; Araki, Y.; Wada, T.; Yoshikawa, O.; Sagawa, T.; Yoshikawa, S.; Imahori, H. *J. Phys. Chem. C* **2009**, *113*, 10798–10806. (j) Angiolillo, P. J.; Lin, V. S.-Y.; Vanderkooi, J. M.; Therien, M. J. *J. Am. Chem. Soc.* **1995**, *117*, 12514–12527. (k) Winters, M. U.; Dahlstedt, E.; Blades, H. E.; Wilson, C. J.; Frampton, M. J.; Anderson, H. L.; Albinsson, B. *J. Am. Chem. Soc.* **2007**, *129*, 4291–4297. (l) Drobizhev, M.; Stepanenko, Y.; Dzenis, Y.; Karotki, A.; Rebane, A.; Taylor, P. N.; Anderson, H. L. *J. Am. Chem. Soc.* **2004**, *126*, 15352–15353. (m) Wong, W.-Y.; Ho, C.-L. *Acc. Chem. Res.* **2010**, *43*, 1246–1256. (n) Ho, C.-L.; Wong, W.-Y. *Coord. Chem. Rev.* **2013**, *257*, 1614–1649. (o) Ho, C.-L.; Wong, W.-Y. *Coord. Chem. Rev.* **2011**, *255*, 2469–2502. (p) Wong, W.-Y.; Harvey, P. D. *Macromol. Rapid Commun.* **2010**, *31*, 671–713. (q) Zhan, H.; Lamare, S.; Ng, A.; Kenny, T.; Guernon, H.; Chan, W.-K.; Djurišić, A. B.; Harvey, P. D.; Wong, W.-Y. *Macromolecules* **2011**, *44*, 5155–5167.
- (3) (a) van Pruissen, G. W. P.; Brebels, J.; Hendriks, K. H.; Wienk, M. M.; Janssen, R. A. *J. Mater. Chem.* **2015**, *25*, 2435–2443. (b) Park, K. H.; Cheon, K. H.; Lee, Y.-J.; Chung, D. S.; Kwon, S.-K.; Kim, Y.-H. *Chem. Commun.* **2015**, *51*, 8120–8122. (c) Areephong, J.; San Juan, R. R.; Payne, A.-J.; Welch, G. C. *New J. Chem.* **2015**, *39*, 5075–5079. (d) Grenier, F.; Aïch, B. R.; Lai, Y.-Y.; Guérette, M.; Holmes, A. B.; Tao, Y.; Wong, W. W. H.; Leclerc, M. *Chem. Mater.* **2015**, *27*, 2137–2143. (e) Elsaywy, W.; Son, M.; Jang, J.; Kim, M. J.; Ji, Y.; Kim, T.-W.; Ko, H.-C.; Elbarbary, A.; Ham, M.-H.; Lee, J.-S. *ACS Macro Lett.* **2015**, *4*, 322–326. (f) Tao, Q.; Xia, Y.; Xu, X.; Hedström, S.; Bäcké, O.; James, D. I.; Persson, P.; Olsson, E.; Inganäs, O.; Hou, L.; Zhu, W.; Wang, E. *Macromolecules* **2015**, *48*, 1009–1016. (g) Brandt, R. G.; Yue, W.; Andersen, T. R.; Larsen-Olsen, T. T.; Hinge, M.; Bundgaard, E.; Krebs, F. C.; Yu, D. *J. Mater. Chem. C* **2015**, *3*, 1633–1639. (h) Liu, Q.; Ho, C.-L.; Lo, Y. H.; Li, H.; Wong, W.-Y. *J. Inorg. Organomet. Polym. Mater.* **2015**, *25*, 159–168. (i) McAfee, S. M.; Topple, J. M.; Payne, A.-J.; Sun, J.-P.; Hill, I. G.; Welch, G. C. *ChemPhysChem* **2015**, *16*, 1190–1202.
- (4) (a) Rawson, J.; Stuart, A. C.; You, W.; Therien, M. J. *J. Am. Chem. Soc.* **2014**, *136*, 17561–17569. (b) Ren, Y.; Hailey, A. K.; Hiszpanski, A. M.; Loo, Y.-L. *Chem. Mater.* **2014**, *26*, 6570–6577. (c) Odajima, T.; Ashizawa, M.; Konosu, Y.; Matsumoto, H.; Mori, T. *J. Mater. Chem. C* **2014**, *2*, 10455–10467. (d) Wang, Q.; Zhang, S.; Ye, L.; Cui, Y.; Fan, H.; Hou, J. *Macromolecules* **2014**, *47*, 5558–5565. (e) Lyu, F.; Park, H.; Lee, S.-H.; Lee, S. H.; Lee, Y.-S. *Chem. Phys. Lett.* **2014**, *610–611*, 388–393. (f) Elsaywy, W.; Kang, H.; Yu, K.; Elbarbary, A.; Lee, K.; Lee, J.-S. *J. Polym. Sci., Part A: Polym. Chem.* **2014**, *52*, 2926–2933. (g) Kim, J.; Han, A.-R.; Hong, J.; Kim, G.; Lee, J.; Shin, T. J.; Oh, J. H.; Yang, C. *Chem. Mater.* **2014**, *26*, 4933–4942. (h) Wu, H.-C.; Benight, S. J.; Chortos, A.; Lee, W.-Y.; Mei, J.; To, J. W. F.; Lu, C.; He, M.; Tok, J. B.-H.; Chen, W.-C.; Bao, Z. *Chem. Mater.* **2014**, *26*, 4544–4551. (i) Li, S.; Ma, L.; Hu, C.; Deng, P.; Wu, Y.; Zhan, X.; Liu, Y.; Zhang, Q. *Dyes Pigm.* **2014**, *109*, 200–205. (j) Kim, G.; Kang, S.-J.; Dutta, G. K.; Han, Y.-K.; Shin, T. J.; Noh, Y.-Y.; Yang, C. *J. Am. Chem. Soc.* **2014**, *136*, 9477–9483. (k) Ho, C.-C.; Chen, C.-A.; Chang, C.-Y.; Darling, S. B.; Su, W.-F. *J. Mater. Chem. A* **2014**, *2*, 8026–8032. (l) Li, S.-G.; Jiang, K.-J.; Huang, J.-H.; Yang, L.-M.; Song, Y.-L. *Chem. Commun.* **2014**, *50*, 4309–4311. (m) Kim, G.; Han, A.-R.; Lee, H. R.; Lee, J.; Oh, J. H.; Yang, C. *Chem. Commun.* **2014**, *50*, 2180–2183. (n) Jung, E. H.; Jo, W. H. *Energy Environ. Sci.* **2014**, *7*, 650–654. (o) Ma, Z.; Sun, W.; Himmelberger, S.; Vandewal, K.; Tang, Z.; Bergqvist, J.; Salleo, A.; Andreasen, J. W.; Inganaes, O.; Andersson, M. R.; Müller, C.; Zhang, F.; Wang, E. *Energy Environ. Sci.* **2014**, *7*, 361–369. (p) Fang, L.; Zhou, Y.; Yao, Y.-X.; Diao, Y.; Lee, W.-Y.; Appleton, A. L.; Allen, R.; Reinspach, J.; Mannsfeld, S. C. B.; Bao, Z. *Chem. Mater.* **2013**, *25*, 4874–4880. (q) Yang, Y.; Wu, R.; Wang, X.; Xu, X.; Li, Z.; Li, K.; Peng, Q. *Chem. Commun.* **2014**, *50*, 439–441. (r) Deng, Y.; Liu, J.; Wang, J.; Liu, L.; Li, W.; Tian, H.; Zhang, X.; Xie, Z.; Geng, Y.; Wang, F. *Adv. Mater.* **2014**, *26*, 471–476.
- (5) (a) Shin, J.; Um, H. A.; Lee, D. H.; Lee, T. W.; Cho, M. J.; Choi, D. H. *Polym. Chem.* **2013**, *4*, 5688–5695. (b) Jung, J. W.; Liu, F.; Russell, T. P.; Jo, W. H. *Energy Environ. Sci.* **2013**, *6*, 3301–3307. (c) Zhuang, W.; Bolognesi, M.; Seri, M.; Henriksson, P.; Gedefaw, D.; Kroon, R.; Jarvid, M.; Lundin, A.; Wang, E.; Muccini, M.; Andersson, M. R. *Macromolecules* **2013**, *46*, 8488–8499. (d) Li, S.; Yuan, J.; Deng, P.; Ma, W.; Zhang, Q. *Sol. Energy Mater. Sol. Cells* **2013**, *118*, 22–29. (e) Dang, D.; Chen, W.; Yang, R.; Zhu, W.; Mammo, W.; Wang, E. *Chem. Commun.* **2013**, *49*, 9335–9337. (f) Ho, C.-C.; Chang, S.-Y.; Huang, T.-C.; Chen, C.-A.; Liao, H.-C.; Chen, Y.-F.; Su, W.-F. *Polym. Chem.* **2013**, *4*, 5351–5360. (g) Chen, M. S.; Niskala, J. R.; Unruh, D. A.; Chu, C. K.; Lee, O. P.; Fréchet, J. M. J. *Chem. Mater.* **2013**, *25*, 4088–4096. (h) Sun, W.; Ma, Z.; Dang, D.; Zhu, W.; Andersson, M. R.; Zhang, F.; Wang, E. *J. Mater. Chem. A* **2013**, *1*, 11141–11144. (i) Karakawa, M.; Aso, Y. *RSC Adv.* **2013**, *3*, 16259–16263. (j) Salvatori, P.; Mosconi, E.; Wang, E.; Andersson, M.; Muccini, M.; De Angelis, F. *J. Phys. Chem. C* **2013**, *117*, 17940–17954. (k) Wu, F.; Yang, H.; Li, C. M.; Qin, *Polym. Adv. Technol.* **2013**, *24*, 945–950. (l) Wan, M.; Zhu, H.; Deng, H.; Jin, L.; Guo, J.; Huang, Y. *J. Polym. Sci., Part A: Polym. Chem.* **2013**, *51*, 3477–3485. (m) Mahmood, K.; Liu, Z.-P.; Li, C.; Lu, Z.; Fang, T.; Liu, X.; Zhou, J.; Lei, T.; Pei, J.; Bo, Z. *Polym. Chem.* **2013**, *4*, 3563–3574. (n) Lei, T.; Dou, J.-H.; Ma, Z.-J.; Liu, C.-J.; Wang, J.-Y.; Pei, J. *Chem. Sci.* **2013**, *4*, 2447–2452. (o) Wang, C.; Zhao, B.; Cao, Z.; Shen, P.; Tan, Z.; Li, X.; Tan, S. *Chem. Commun.* **2013**, *49*, 3857–3859. (p) Yan, Z.; Sun, B.; Li, Y. *Chem. Commun.* **2013**, *49*, 3790–3792. (q) Sonar, P.; Tan, H.-S.; Sun, S.; Lam, Y. M.; Dodabalapur, A. *Polym. Chem.* **2013**, *4*, 1983–1994. (r) Grenier, F.; Berrouard, P.; Pouliot, J.-R.; Tseng, H.-R.; Heeger, A. J.; Leclerc, M. *Polym. Chem.* **2013**, *4*, 1836–1841. (s) Yassin, A.; Leriche, P.; Allain, M.; Roncali, J. *New J. Chem.* **2013**, *37*, 502–507. (t) Kim, D. H.; Ayzner, A. L.; Appleton, A. L.; Schmidt, K.; Mei, J.; Toney, M. F.; Bao, Z. *Chem. Mater.* **2013**, *25*, 431–440. (u) Graham, K. R.; Stalder, R.; Wieruszewski, P. M.; Patel, D. G.; Salazar, D. H.; Reynolds, J. R. *ACS Appl. Mater. Interfaces* **2013**, *5*, 63–71.
- (6) Wang, X.; Fortin, D.; Brisard, G.; Harvey, P. D. *Macromol. Rapid Commun.* **2014**, *35*, 992–997.

- (7) Mai, C.-L.; Huang, Y.-L.; Chiu, C.-L.; Lin, H.-Y.; Lin, Y.-S.; Yeh, C.-Y. *J. Chin. Chem. Soc.* **2013**, *60*, 986–990.
- (8) (a) Wang, X.; Kenny, T.; Fortin, D.; Aly, S. M.; Brisard, G.; Harvey, P. D. *Organometallics* **2015**, *34*, 1567–1581. (b) Aly, S. M.; Kenny, T.; Lamare, S.; Harvey, P. D. *J. Inorg. Organomet. Polym. Mater.* **2015**, *25*, 118–125. (c) Kenny, T.; Aly, S. M.; Brisard, G.; Fortin, D.; Harvey, P. D. *Macromol. Rapid Commun.* **2013**, *34*, 511–515. (d) Kenny, T.; Lamare, S.; Aly, S. M.; Fortin, D.; Brisard, G.; Harvey, P. D. *Inorg. Chem.* **2012**, *51*, 13081–13095. (e) Lamare, S.; Aly, S. M.; Fortin, D.; Harvey, P. D. *Chem. Commun.* **2011**, 47, 10942–10944. (f) Gagnon, K.; Aly, S. M.; Fortin, D.; Abd-El-Aziz, A. S.; Harvey, P. D. *J. Inorg. Organomet. Polym. Mater.* **2009**, *19*, 28–34. (g) Fortin, D.; Clément, S.; Gagnon, K.; Bérubé, J.-F.; Stewart, M. P.; Geiger, W. E.; Harvey, P. D. *Inorg. Chem.* **2009**, *48*, 446–454. (h) Gagnon, K.; Mohammed Aly, S.; Brisach-Wittmeyer, A.; Bellows, D.; Bérubé, J.-F.; Caron, L.; Abd-El-Aziz, A. S.; Fortin, D.; Harvey, P. D. *Organometallics* **2008**, *27*, 2201–2214.
- (9) Kenny, T.; Aly, S. M.; Fortin, D.; Harvey, P. D. *Chem. Commun.* **2012**, 48, 11543–11545.
- (10) (a) Ranjan, K. R.; Singh, A.; Banerjee, A.; Singh, B. *J. Coord. Chem.* **2011**, *64*, 1411–1425. (b) Han, M.; Bie, H.; Nikles, D. E.; Warren, G. W. *J. Polym. Sci., Part A: Polym. Chem.* **2000**, *38*, 2893–2899. (c) Wang, X.; Fortin, D.; Brisard, G.; Harvey, P. D. *Chem. Commun.* **2014**, 50, 350–352.
- (11) Gaina, C.; Gaina, V.; Stoleriu, A.; Sava, M.; Chiriac, C. *Des. Monomers Polym.* **1998**, *1*, 315–325.
- (12) Cheng, F.; Adronov, A. *Chem. - Eur. J.* **2006**, *12*, 5053–5059.
- (13) Estrada, L. A.; Liu, D. Y.; Salazar, D. H.; Dyer, A. L.; Reynolds, J. R. *Macromolecules* **2012**, *45*, 8211–8220.
- (14) Lee, S. K.; Yang, W. J.; Choi, J. J.; Kim, C. H.; Jeon, S. J.; Cho, B. R. *Org. Lett.* **2005**, *7*, 323–326.
- (15) Abou-Elkhair, R. A. I.; Netzels, T. L. *Nucleosides, Nucleotides Nucleic Acids* **2005**, *24*, 85–110.
- (16) Connelly, N. G.; Geiger, W. E. *Chem. Rev.* **1996**, *96*, 877–910.
- (17) (a) Figueiredo, T. L. C.; Johnstone, R. A. W.; SantAna Sørensen, A. M. P.; Burget, D.; Jacques, P. *Photochem. Photobiol.* **1999**, *69*, 517–528. (b) Webster, S.; Odom, S. A.; Padilha, L. A.; Przhonska, O. V.; Peceli, D.; Hu, H.; Nootz, G.; Kachkovski, A. D.; Matichak, J.; Barlow, S.; Anderson, H. L.; Marder, S. R.; Hagan, D. J.; Van Stryland, E. W. *J. Phys. Chem. B* **2009**, *113*, 14854–14867.
- (18) Flack, H. D.; Blanc, E.; Schwarzenbach, D. *J. Appl. Crystallogr.* **1992**, *25*, 455–459.
- (19) Gabe, E. J.; Le Page, Y.; Charland, J.-P.; Lee, F. L.; White, P. S. *J. Appl. Crystallogr.* **1989**, *22*, 384–387.
- (20) Sheldrick, G. M. *SHELXS-97*; University of Göttingen: Göttingen, Germany, 1997, Release 97–2.
- (21) Frisch, M. J.; Trucks, G. W.; Schlegel, H. B.; Scuseria, G. E.; Robb, M. A.; Cheeseman, J. R.; Zakrzewski, V. G.; Montgomery, J. A., Jr.; Stratmann, R. E.; Burant, J. C.; Dapprich, S.; Millam, J. M.; Daniels, A. D.; Kudin, K. N.; Strain, M. C.; Farkas, O.; Tomasi, J.; Barone, V.; Cossi, M.; Cammi, R.; Mennucci, B.; Pomelli, C.; Adamo, C.; Clifford, S.; Ochterski, J.; Petersson, G. A.; Ayala, P. Y.; Cui, Q.; Morokuma, K.; Malick, D. K.; Rabuck, A. D.; Raghavachari, K.; Foresman, J. B.; Cioslowski, J.; Ortiz, J. V.; Baboul, A. G.; Stefanov, B. B.; Liu, G.; Liashenko, A.; Piskorz, P.; Komaromi, I.; Gomperts, R.; Martin, R. L.; Fox, D. J.; Keith, T.; Al-Laham, M. A.; Peng, C. Y.; Nanayakkara, A.; Gonzalez, C.; Challacombe, M.; Gill, P. M.; Johnson, B. G.; Chen, W.; Wong, M. W.; Andres, J. L.; Head-Gordon, M.; Replogle, E. S.; Pople, J. A. *Gaussian 09, Revision D.01*. Gaussian, Inc.: Wallingford, CT, 2009.
- (22) Hohenberg, P.; Kohn, W. *Phys. Rev.* **1964**, *136*, B864–B871.
- (23) Kohn, W.; Sham, L. J. *Phys. Rev.* **1965**, *140*, A1133–A1138.
- (24) Salahub, D. R.; Zerner, M. C. *The Challenge of d and f Electrons*; American Chemical Society: Washington, D.C., 1989.
- (25) Parr, R. G.; Yang, W. *Density-functional theory of atoms and molecules*; Oxford Univ. Press: Oxford, U.K., 1989.
- (26) Stratmann, R. E.; Scuseria, G. E.; Frisch, M. J. *J. Chem. Phys.* **1998**, *109*, 8218–8224.
- (27) Bauernschmitt, R.; Ahlrichs, R. *Chem. Phys. Lett.* **1996**, *256*, 454–464.
- (28) Casida, M. E.; Jamorski, C.; Casida, K. C.; Salahub, D. R. *J. Chem. Phys.* **1998**, *108*, 4439–4449.
- (29) Becke, A. D. *J. Chem. Phys.* **1993**, *98*, 5648–5652.
- (30) Lee, C.; Yang, W.; Parr, R. G. *Phys. Rev. B: Condens. Matter Mater. Phys.* **1988**, *37*, 785–789.
- (31) Miehlich, B.; Savin, A.; Stoll, H.; Preuss, H. *Chem. Phys. Lett.* **1989**, *157*, 200–206.
- (32) Binkley, J. S.; Pople, J. A.; Hehre, W. J. *J. Am. Chem. Soc.* **1980**, *102*, 939–947.
- (33) Gordon, M. S.; Binkley, J. S.; Pople, J. A.; Pietro, W. J.; Hehre, W. J. *J. Am. Chem. Soc.* **1982**, *104*, 2797–2803.
- (34) Pietro, W. J.; Francl, M. M.; Hehre, W. J.; Defrees, D. J.; Pople, J. A.; Binkley, J. S. *J. Am. Chem. Soc.* **1982**, *104*, 5039–5048.
- (35) Dobbs, K. D.; Hehre, W. J. *J. Comput. Chem.* **1986**, *7*, 359–378.
- (36) Dobbs, K. D.; Hehre, W. J. *J. Comput. Chem.* **1987**, *8*, 861–879.
- (37) Dobbs, K. D.; Hehre, W. J. *J. Comput. Chem.* **1987**, *8*, 880–893.
- (38) Godbout, N.; Salahub, D. R.; Andzelm, J.; Wimmer, E. *Can. J. Chem.* **1992**, *70*, 560–571.
- (39) SBKJJC ECP EMSL Basis Set Exchange Library.
- (40) Stevens, W. J.; Krauss, M.; Basch, H.; Jasien, P. G. *Can. J. Chem.* **1992**, *70*, 612–630.
- (41) O'boyle, N. M.; Tenderholt, A. L.; Langner, K. M. *J. Comput. Chem.* **2008**, *29*, 839–845.
- (42) Namazian, M. *J. Mol. Struct.: THEOCHEM* **2003**, *664-665*, 273–278.
- (43) Lowry, M. S.; Hudson, W. R.; Pascal, R. A., Jr.; Bernhard, S. J. *Am. Chem. Soc.* **2004**, *126*, 14129–14135.
- (44) LeCours, S. M.; DiMagno, S. G.; Therien, M. J. *J. Am. Chem. Soc.* **1996**, *118*, 11854–11864.
- (45) Jiang, F.-L.; Fortin, D.; Harvey, P. D. *Inorg. Chem.* **2010**, *49*, 2614–2623.
- (46) Soliman, A. M.; Fortin, D.; Zysman-Colman, E.; Harvey, P. D. *Chem. Commun.* **2012**, 48, 6271–6273.
- (47) Susumu, K.; Therien, M. J. *J. Porphyrins Phthalocyanines* **2015**, *19*, 205–218.
- (48) Clément, S.; Goudreault, T.; Bellows, D.; Fortin, D.; Guyard, L.; Knorr, M.; Harvey, P. D. *Chem. Commun.* **2012**, 48, 8640–8642.
- (49) Harvey, P. D.; Stern, C.; Guillard, R. *3rd Handbook on Porphyrins and Phthalocyanines*; Kadish, K., Guillard, R., Smith, K. M., Eds.; World Science: Singapore, 2011, Vol. 11, pp 1–179.
- (50) Harvey, P. D. *2nd Handbook on Porphyrins and Phthalocyanines*; Kadish, K., Guillard, R., Smith, K. M., Eds.; Elsevier: Amsterdam, 2003, Chapter 113, pp 63–249.
- (51) (a) Perchanova, M.; Kurreck, H.; Berg, A. *J. Phys. Chem. A* **2015**, *119*, 8117. (b) Kichigina, A. O.; Ionkin, V. N.; Ivanov, A. I. *J. Phys. Chem. B* **2013**, *117*, 7426–7435. (c) Okamoto, K.; Fukuzumi, S. *J. Phys. Chem. B* **2005**, *109*, 7713–7723.
- (52) (a) Zhao, P.; Huang, J. W.; Xu, L. C.; Ma, L.; Ji, L. N. *Spectrochim. Acta, Part A* **2011**, *78*, 437–442. (b) Giribabu, L.; Reeta, P. S.; Kanaparthi, R. K.; Srikanth, M.; Soujanya, Y. *J. Phys. Chem. A* **2013**, *117*, 2944–2951.
- (53) Yu, H.-Z.; Baskin, J. S.; Zewail, A. H. *J. Phys. Chem. A* **2002**, *106*, 9845–9854.
- (54) (a) Khairutdinov, R. F.; Serpone, N. *J. Phys. Chem. B* **1999**, *103*, 761–769. (b) Kärnbratt, J.; Gilbert, M.; Sprafke, J. K.; Anderson, H. L.; Albinsson, B. *J. Phys. Chem. C* **2012**, *116*, 19630–19635.